Short title: Chlamydomonas ribosomes and cell cycle under ion stress

Correspondence:

Tobias Wunder

Plant Biochemistry and Physiology

LMU Munich

Großhaderner Str. 2-4, 82152 Planegg-Martinsried, Germany

Email: tobias.wunder@lmu.de

Conserved and Lineage-Specific Roles of KEA-Mediated Ion Homeostasis in *Chlamydomonas*

Tobias Wunder[*+a], Leon Eulitz[a], Luis Kramer[a], Zahin Mohd Ali[b], Matthias Ostermeier[c], Charlott Leu[d], Beata Szulc[a], Lorenz J. Holzner[a], Jonas Fechter[a], Francesco Padovani[e], Benjamin Brandt[a], Philipp Girr[f], Jing Tsong Teh[c], Susanne Mühlbauer[a], Clara Sotos[g], Max Angstenberger[h], Luke C. M. Mackinder[f], Kurt M. Schmoller[e], Joachim O. Rädler[d], Jörg Nickelsen[c], Jan de Vries[b], Hans-Henning Kunz[+a]

[a] Plant Biochemistry and Physiology, LMU München, Großhaderner Straße 2-4, 82152, Martinsried-Planegg, Germany.

[b] Institute of Microbiology and Genetics, Göttingen Center for Molecular Biosciences (GZMB), Campus Institute Data Science (CIDAS), Department of Applied Bioinformatics, University of Göttingen, Goldschmidtstr. 1, 37077 Göttingen, Germany

[c] Molecular Plant Science, LMU Munich, Großhaderner Straße 2-4, 82152 Planegg-Martinsried, Germany.

[d] Faculty of Physics and Center for NanoScience, Ludwig-Maximilian-University, Geschwister-Scholl-Platz 1, D-80539 Munich, Germany

[e] Institute of Functional Epigenetics, Molecular Targets and Therapeutics Center, Helmholtz Zentrum Muenchen, 85764 Neuherberg, Germany

[f] Centre for Novel Agricultural Products (CNAP), Department of Biology, University of York, Heslington, York YO10 5DD, UK.

[g] Institute for Integrative Biology of the Cell (I2BC), Université Paris-Saclay, CEA, CNRS, 91198 Gif-sur-Yvette cedex, France.

[h] Institute of Molecular Biosciences, Goethe University Frankfurt, 60438 Frankfurt, Germany

*Corresponding author: Tobias Wunder, tobias.wunder@lmu.de

[+]Senior authors: Tobias Wunder, tobias.wunder@lmu.de, Hans-Henning Kunz, kunz@lmu.de

Keywords: photosynthesis, ion balance, rRNA processing, cell cycle, microalgae, chloroplast

One-sentence summary

Disruption of KEA-mediated chloroplast ion homeostasis in *Chlamydomonas reinhardtii* reveals conserved and lineage-specific control of plastid rRNA processing and cell cycle progression.

Footnotes:

Author Contributions

T.W. and H.-H.K. conceived research idea and wrote the manuscript. T.W. cloned constructs, isolated algal and plant mutants, performed most experiments, analyzed data, and designed the figures. L.E. performed single-cell imaging, analyzed image data, designed figures, and wrote sections. L.J.H. conducted TXRF and analyzed elemental data. C.S. generated plant mutants and helped with element analysis. L.K. and B.S. performed and assisted in RNA and growth experiments. J.F. carried out RNA-blots. M.A. isolated algal mutants. F.P. and K.M.S. supported analysis of single-cell imaging data. M.O. performed transmission electron microscopy. B.B. assisted with RNA-seq data analysis and visualization. P.G. and L.C.M.M. recombineered plasmids. Z.M.A. and J.dV. performed cross-species gene network analyses. C.L. and J.O.R. designed and fabricated hydrogel flow-cell chips. S.M. provided illustration. J.T.T. and J.N. designed and carried out initial CRISPR/Cas9. All authors assisted in editing the manuscript.

Abstract

In Arabidopsis (*Arabidopsis thaliana*), seamless plastid gene expression and development depend on finely balanced ion homeostasis across the inner envelope (IE) membrane, maintained by the K^+/H^+ antiporters AtKEA1/2. To assess whether these functions are retained across mono- and polyplastidic representatives of the green lineage, we studied CrKEA1, the sole IE KEA homolog in the unicellular alga Chlamydomonas (*Chlamydomonas reinhardtii*). Using CRISPR/Cas9, we generated a *kea1* knockout mutant that exhibits impaired photoautotrophic growth, chloroplast deformation, and photoinhibition. Transcriptomics revealed strong induction of ribosome biogenesis genes and reduced abundance of transcripts associated with cell and plastid division. Further RNA analyses confirmed defects in stromal rRNA maturation of *kea1*, paralleling observations from Arabidopsis *kea1kea2* mutants. Expression of *CrKEA1* in Arabidopsis rescued growth and rRNA maturation in *kea1kea2*, demonstrating functional continuity after the ancient divergence between the two lineages. Cross-species transcriptomic comparisons further revealed that *KEA* loss elicits both shared and species-specific transcriptional responses: *PhANG* repression was conserved between algae and plants, whereas activation of the chloroplast unfolded protein response (cpUPR) and reduced expression of genes tied to cell-cycle and plastid fission occurred only in Chlamydomonas. Single-cell time-lapse imaging confirmed that *kea1* exhibits an increased rate of aberrant cytokinesis, unequal division, and cell death. Our findings demonstrate that while IE KEA transporters fulfill conserved roles in maintaining the conditions for a functional plastid gene expression machinery, their integration into broader cellular networks has diverged between algae and land plants. This underscores a lineage-dependent tuning of plastid-to-nucleus communication shaped by organismal complexity and plastid number.

Introduction

A balanced ionic milieu is essential for plastid biogenesis and function. In Arabidopsis (*Arabidopsis thaliana)*, disruption of the inner envelope (IE) K^+/H^+ antiporters KEA1 and KEA2 produces a virescent phenotype i.e., pale young leaves that eventually develop into green photosynthesizing tissue (Kunz et al., 2014). Subsequent work revealed that the essential role of KEA1/2 in plastid integrity and photosynthetic performance is linked to plastid gene expression and rRNA maturation (DeTar et al., 2021). These findings demonstrate a strong connection between organellar ion homeostasis and chloroplast biogenesis.

Dissecting this link mechanistically in plant cells is complicated due to their multicellular organization and polyplastidy: Plants typically harbor cells with dozens of plastids displaying heterogeneous behavior depending on tissue context and developmental stage (Knoblauch et al., 2024; Renna et al., 2025). This cellular heterogeneity makes it challenging to distinguish direct, plastid-autonomous consequences of ion imbalance from secondary effects at the tissue or organismal level.

Interestingly, unicellular algae maintain a single plastid per cell. de Vries and Gould, 2018 described the evolutionary framework of the "monoplastidic bottleneck", which posits that the ancestor of all Archaeplastida (Figure 1A) passed through a stage where plastid and host cell division were strictly synchronized. The unicellular green algae Chlamydomonas (*Chlamydomonas reinhardtii*), with its single cup-shaped chloroplast, represents a bona fide example of this ancestral state. In contrast, land plants such as Arabidopsis, have since evolved polyplastidy and decoupled plastid division from the nuclear cycle. Thus, Chlamydomonas is an ideal model to study the direct relation between plastid physiology, cell growth, and division, as each cell depends on a single plastid for both metabolism and successful cytokinesis.

Despite around a billion years of divergence between chlorophyte algae and streptophyte plants (Figure 1A), IE KEA transporters are conserved across the green lineage, and orthologs are present in green algae (Kunz et al., 2024). This conservation raises the question of whether KEA proteins maintain mechanistic similarity or whether their roles have been rewired in line with lineage-specific cellular contexts.

In this study, we employ Chlamydomonas for an initial investigation into how KEA-mediated ion transport across plastid envelope membranes influences the organelle's function, cell physiology, and cell cycle in a unicellular, monoplastidic organism. By combining mutant analyses, transcriptome comparisons with Arabidopsis (DeTar et al., 2021), and cross-species complementation, we show that KEA function is a prerequisite for maintaining the integrity of ribosome biogenesis. Leveraging the complementary strengths of a multicellular polyplastidic plant and a unicellular monoplastidic alga (Gutman and Niyogi, 2004), we provide evidence that KEA's importance for plastid gene expression is deeply conserved, while its cellular consequences are shaped by lineage-specific developmental context.

Results

Generation of CrKEA1 knock-out and complementation lines for subcellular localization studies of CrKEA1

KEA genes are conserved from green algae to angiosperms (Chanroj et al., 2012). Through amino acid sequence homology analysis, we identified Cre04.g220200 (*CrKEA1*) as the only homolog of inner envelope (IE) K^+/H^+ exchangers AtKEA1/2 from Arabidopsis in Chlamydomonas (see alignment, Supplemental Figure S1). The conserved monovalent cation/proton antiporter 2 (CPA2) domain and the regulatory K^+ transport and NAD-binding (KTN) domain share 56% sequence identity and 71% similarity between plant and algae KEA1. In contrast, the extended N-terminal region (~500 amino acids) — a characteristic feature of all IE KEAs that includes a coiled-coil domain embedded within a highly disordered segment (Chanroj et al., 2012; Bölter et al., 2020) — is far less conserved, showing only 13% identity and 29% similarity.

To investigate CrKEA1 function in Chlamydomonas, we initially generated a CrKEA1 antibody (Supplemental Figure S2, A-C) with a detection sensitivity against its antigen (CrKEA1_aa94-337) in the picogram range (Supplemental Figure S2D). We attempted to utilize mutant strain LMJ.RY0402.187220, which at the time was the only CLiP insertion line in the *CrKEA1* locus (Li et al., 2016). However, protein expression in wild type (WT) cells and LMJ.RY0402.187220 was clearly detectable at an apparent size of ~120 kDa (calculated size 108 kDa for full length size, without estimated chloroplast targeting peptide, cTP, ~101 kDa), confirming functionality of the CrKEA1 antibody with Chlamydomonas protein extracts but also that the CLiP line had not lost CrKEA1 (Supplemental Figure S2E). We therefore turned towards an established CRISPR/Cas9 protocol (Kelterborn et al., 2022) to generate *CrKEA1* knock-out strains ourselves. We successfully isolated a *kea1* mutant with a stop codon insertion in exon 19 (Figure 1B), which was confirmed by PCR screening and Sanger sequencing (Supplemental Figure S3, A-D; Supplemental Table S1). Immunoblotting further verified the loss of full-length CrKEA1 (Figure 1C; Supplemental Figure S3E). Lastly, we sequenced the genome of *kea1*, which allowed us to annotate the entire insertion site (Supplemental Figure S3F, Figure S4) and to verify the absence of additional CRISPR/Cas9-mediated insertions in this background.

To analyze the subcellular localization of CrKEA1, we generated complementation lines by transforming *kea1* with *CrKEA1* fused to a *YFP* at the C-terminus under the control of its native

104 promoter. Immunoblotting with the CrKEA1 antibody confirmed CrKEA1-YFP expression,
105 detecting a band at ~140 kDa that migrated ~30 kDa larger compared to the endogenous signal
106 (Figure 1C; Supplemental Figure S5A) — consistent with the added YFP tag (calculated 138 kDa
107 full length, 132 kDa without cTP). Subsequently, we performed fluorescence microscopy and
108 found the YFP fluorescence signal to emerge from the membrane that surrounds the chlorophyll
109 autofluorescence. This confirms that CrKEA1, consistent with its plant homologs, resides in the
110 plastid envelope membrane (Figure 1D; Supplemental Figure S5B).

111 *Hampered growth upon loss of CrKEA1 in kea1 strains*

112 Chlamydomonas can grow hetero- and mixotrophically on acetate-supplemented TAP
113 medium or autotrophically in HSM medium, relying entirely on CO_2 fixation via RuBisCO (Sager
114 and Zalokar, 1958; Harris et al., 2009; Grossman et al., 2010; Lauersen et al., 2016). To assess the
115 impact of CrKEA1 loss, we tested our strains under different growth conditions at 23°C. Initially,
116 we employed agar plates and liquid cultures at 25 µmol photons m^{-2} s^{-1} (hereafter abbreviated as
117 µE) of light to avoid stress exposure of potentially affected mutants. On TAP plates, slightly
118 decreased growth was observed for *kea1* only at $\leq 10^4$ spotted cells. This effect was more prevalent
119 if mutant cells were grown autotrophically on HSM plates. Here, genotype-specific differences
120 already emerged at cell numbers between 10^6 and 10^5. In both cases, the expression of CrKEA1-
121 YFP in the *kea1* background restored WT growth behavior (Figure 1E). The slow growth of *kea1*
122 cells replicated well in liquid cultures. Again, the absence of acetate clearly exacerbated this effect;
123 even after nine days of culturing, *kea1* reached only half the cell number as WT and the *CrKEA1-*
124 *YFP* complemented the *kea1* strain (Figure 1F).

125 *Transmission electron microscopy (TEM) reveals deformed chloroplasts and swollen cells in kea1*

126 To learn more about the slowly growing mutant cells, we examined cell and chloroplast
127 ultrastructure in WT, *kea1*, and *CrKEA1–YFP* complementation lines by transmission electron
128 microscopy (TEM; Figure 1G, H; Supplemental Figure S5C). WT and *CrKEA1–YFP*
129 complemented *kea1* cells consistently displayed the canonical, cup-shaped chloroplast with well-
130 defined lobes, regular thylakoid lamellae, and a distinct pyrenoid matrix. In contrast, *kea1* cells
131 had a strikingly different appearance under these conditions: 1) the characteristic cup morphology
132 of the chloroplast was lost i.e., plastids assumed a more spheroidal (globular) shape, without the
133 pronounced lobes seen in WT and complemented strains; 2) thylakoid bundles within spherical

134 chloroplasts were highly disordered and lost, in contrast to the lamellar arrays of the WT; 3) the
135 pyrenoid, a critical hub for carbon fixation (Catherall et al., 2025), was disintegrated in the majority
136 of *kea1* cells, suggesting that CrKEA1 permitted ion exchange may be essential for proper
137 pyrenoid assembly or stability; 4) Finally, cell and plastid size variation was markedly increased
138 in the mutant population, pointing to a loss of volume homeostasis. Together, these observations
139 suggest a role of CrKEA1 in maintaining chloroplast shape, thylakoid organization, pyrenoid
140 integrity, and by extension, cellular architecture (Figure 1G-H; Supplemental Figure S5C).

141 *kea1 mutant cells exhibit deviant ion content*

142 To assess whether the growth defects of the *kea1* mutant are associated with disturbed ion
143 homeostasis, we quantified the elemental composition of whole cells using total reflection X-ray
144 fluorescence (TXRF; Holzner et al., 2025). WT, *kea1*, and the complementation line (*CrKEA1-*
145 *YFP* in *kea1*) were analyzed from TAP cultures grown at 25 µE. Overall, elemental profiles per
146 cell were close to the values reported previously (Merchant et al., 2020; Schmollinger et al., 2021;
147 Figure 2). Potassium (K^+) content was higher in *kea1* than in WT, while several other elements
148 also showed elevated values, consistent with the larger average cell size of the mutants. The
149 complementation line displayed intermediate K^+ levels between mutant and WT. Because IE KEA-
150 type transporters mediate K^+ export from the chloroplast and not from the cell, even a severe
151 internal ionic imbalance may only modestly impact whole-cell K^+ accumulation.

152 *Loss of CrKEA1 results in a light-dependent decrease in photosynthetic performance*

153 To investigate whether the observed growth defects correlate with impaired photosynthetic
154 performance, we recorded electron transport rates (ETR) during step-wise light intensity
155 (photosynthetically active radiation; PAR) increases. Interestingly, once light intensities surpassed
156 the moderate range ≥80 PAR, *kea1* cells revealed lower ETR indicative of higher light
157 susceptibility than WT and the complementation line (Figure 3A). A similar effect was observed
158 in drop cultures. While the maximum quantum efficiency of PSII (F_v/F_m) did not differ between
159 genotypes at 0–20 µE, stepwise increases in light intensity (every hour) caused a stronger decline
160 in F_v/F_m in *kea1* compared to WT and the complementation line (Figure 3B).

161 For additional insight, we established a light intensity shift routine for liquid cultures.
162 Initially, F_v/F_m was determined in all three genotypes grown at 25 µE either in HSM or TAP media.
163 Regardless of the growth media used, no clear differences emerged across the strains. However, if

164 the same genotypes were shifted to standard moderate light conditions (100 µE; Bialevich et al.,
165 2022) for 24 h, a clear F_v/F_m drop was noticeable for the mutant (Figure 3C). Subsequent
166 incubation for 24 h at 25 µE restored F_v/F_m to baseline levels.

167 In summary, *kea1* mutants are highly light sensitive and show clear photosynthetic defects,
168 which are fully rescued by *CrKEA1-YFP* expression, confirming loss of *CrKEA1* as the causative
169 mutation. While low light intensities (25 µE) are mostly permissive for *kea1*, PSII efficiency
170 declines sharply under moderate light (~100 µE).

171 *Flow cytometry shows increased cell sizes for kea1 shifted from low to moderate light*

172 Next, we examined the response of TAP and HSM cultures to the light shift using flow
173 cytometry (Figure 3D; Supplemental Figure S6). Regardless of the growth medium, *kea1* cells
174 were slightly larger in size based on FSC-A values at low light (25 µE). 48 h after the shift to
175 moderate light (100 µE), cell size increased for both media across all genotypes. However, *kea1*
176 cultures showed the strongest increase in cell size and broadening of the size distribution. After
177 48 h of moderate light treatment, calibration indicated average volume increases of 19% in TAP
178 and 23% in HSM for WT, 9% in TAP and 19% in HSM for the *CrKEA1-YFP* line, and 97% in
179 TAP and 67% in HSM for *kea1* (Supplemental Table S2). Using SSC-A as a proxy for cell
180 complexity, changes in the *kea1* mutant (82%) by far exceeded those in WT (-4%) and the
181 complemented line (6%) under TAP conditions. A similar trend was observed in HSM, with
182 complexity increases of 52% for *kea1*, 19% for WT, and 4% for the *CrKEA1-YFP* line
183 (Supplemental Table 3).

184 *Transcriptome profiling during light acclimation reveals that the absence of KEA1 alters ribosome*
185 *biogenesis, plastid fission and cell cycle regulation*

186 Given the impaired physiological performance of *kea1* mutant cells upon shift into
187 moderate light, we sought to identify biological processes affected by the loss of *CrKEA1* through
188 characterizing the underlying transcriptional responses. To this end, we performed RNA
189 sequencing (RNA-seq) on cultures subjected to the established light shift regime. Cells grown
190 under low light (LL, 25 µE) were exposed to moderate light (ML, µE) for 8 h, followed by a 24 h
191 low-light recovery phase (RL, 25 µE) (Figure 4A). The experiment was set up with TAP medium
192 to ensure that *kea1* cells experience stress but not the exacerbated defects observed in HSM. Ribo-

193 depleted libraries were prepared to capture the full extent of transcriptional changes, including
194 organellar transcripts.

195 For physiological validation of the light treatment, we again recorded F_v/F_m at each
196 sampling point. While there was no genotype-specific difference at the onset of the experiments
197 i.e., at 25 µE, only 8 h at 100 µE induced clear PSII photoinhibition (F_v/F_m drop) in *kea1* mutants.
198 By contrast, WT cells readily acclimated to the changing light regime (Figure 4A; Supplemental
199 Figure S7A). Following the RL phase, PSII quantum yield was fully restored in all genotypes..

200 Multidimensional scaling (MDS) showed tight clustering of replicates (n=4) and a stronger
201 genotype separation under ML (Supplemental Figure S7B). Consistent with this, the number of
202 significantly differentially expressed genes (DEGs, adjusted p-value < 0.05) under LL (1419
203 DEGs) went up >6-fold under ML (7632 DEGs) but back down at RL conditions (1370 DEGs)
204 (Figure 4A; Supplemental Table S4). In addition, ML DEGs were more strongly deregulated, i.e.,
205 more DEGs above the $|\log_2 FC| \geq 1$ threshold than under other light conditions.

206 Gene Ontology (GO) enrichment analyses highlighted a coordinated shift in cellular
207 programs under ML (Figure 4B; Supplemental Table S5): Upregulated DEGs were strongly
208 enriched for *ribosome biogenesis*, including *rRNA processing*. Both categories contained cytosolic
209 and plastid ribosome biogenesis components. Downregulated categories included *cell cycle*, *DNA*
210 *replication*, *chromatin organization*, and *microtubule-based processes*, which to some degree are
211 intertwined.

212 Consistent with this, a detailed analysis of transcript changes in the tested conditions
213 revealed a broad upregulation of ribosome-related genes when *kea1* cells were exposed to
214 moderate light (Figure 4C). By contrast, cell cycle–related genes were by and large downregulated
215 in *kea1* cells under these light conditions (Figure 4D). While *CDKA1*, the major driver of the G1/S
216 transition (Tulin and Cross, 2014), was unchanged, multiple key regulators of the Chlamydomonas
217 cell cycle were expressed below WT-level in *kea1*: Expression of genes controlling S/M transitions
218 by blocking spindle formation was strongly decreased, including *CDKB1(2)* and its activating
219 cyclins (*CYCA1*, *CYCB1*). Three of the D-type cyclins, which mediate G1/S entry (Bisova et al.,
220 2005), were mildly reduced (~2-fold for *CYCD3, 5*). In addition, transcript accumulation for both
221 *CDKG1*, which becomes induced when cells reach sufficient size for division (Li et al., 2016), and
222 for *MAT3*, a retinoblastoma homolog regulating the commitment to division (Umen and

223 Goodenough, 2001), were slightly diminished. Together, these changes provide evidence that the
224 cell cycle entry and S/M cycling might be affected in the *kea1* mutants (Supplemental Figure S7E).
225 Interestingly, most transcripts associated with the GO term *plastid fission* were markedly
226 reduced in light-shifted *kea1* cells (Figure 4E), suggesting a link between KEA1 function in the
227 plastid envelope membrane and chloroplast division control in algae.

228 *The absence of KEA1 triggers PhANG suppression but an induction of PGE and protein*
229 *homeostasis genes*

230 Arabidopsis *kea1kea2* mutants display delayed chloroplast biogenesis caused by activation
231 of GUN1-dependent retrograde signaling, which suppresses the expression of GOLDEN2-LIKE
232 transcription factors and their downstream gene cluster of photosynthesis-associated nuclear genes
233 (PhANGs; DeTar et al., 2021). Hence, we also curated a PhANG list for Chlamydomonas.
234 Interestingly, *kea1* showed a clear repression of genes encoding for light-harvesting complexes,
235 photosystem subunits, and chlorophyll biosynthesis enzymes under ML (Figure 4F), which is
236 reminiscent of the response described for *kea1kea2* plant mutants (DeTar et al., 2021).
237 Furthermore, among downregulated genes, also photosynthesis-related GO terms were enriched
238 in the Chlamydomonas *kea1* mutant (Figure 4B). By contrast, plastid-encoded photosynthesis
239 genes were largely unaffected, though transcripts for plastid transcription/translation components
240 (e.g., RNA polymerase subunits, ribosomal proteins), essential for plastid gene expression (PGE),
241 were elevated in *kea1* compared to WT (Figure 4G; Supplemental Figure S7G). This suggests that
242 the photosynthetic decline may not only arise from a transcriptional repression within the plastid,
243 but in addition from defective translation, consistent with the general enrichment of ribosome
244 biogenesis transcripts.
245 Other DEG categories were more selective. Chloroplast-encoded genes for chlorophyll
246 biosynthesis were unchanged in *kea1* (Supplemental Figure S7G). Likewise, *HMOX* and *GUN4*,
247 which regulate tetrapyrrole and bilin synthesis relevant for retrograde signaling in
248 Chlamydomonas (Duanmu et al., 2013), were unaffected. However, bilin-synthesis gene *PCYA*
249 was upregulated under ML (Figure 3H). Chlamydomonas lacks close *GOLDEN2-LIKE*
250 *transcription factor* homologs and probably relies mainly on a bilin-derived retrograde signaling
251 pathway to repress PhANGs and facilitate acclimation (Duanmu et al., 2013; Richter et al., 2023).

252 Hence, the observed *PCYA* induction likely contributes to the reduced PhANG expression
253 observed in *kea1*.
254 Next, we examined nuclear genes implicated in protein homeostasis, ROS defense, and
255 photoprotection (Figure 4H). Plastid-encoded quality control proteins, namely *PsbN* involved in
256 PSII repair and the proteases *ClpP* and *FtsH*, were mildly upregulated in *kea1* under ML, while
257 nuclear-encoded PSII repair factors (*HCF136*, *TerC1*, *ALB3*, *PsbW*, *PsbY*; Plöchinger 2016)
258 showed no consistent change with a tendency for down-regulation. Several ROS-related genes
259 (*GPX5*, *MBS*, *SOR1*, *VTC2*) were upregulated in the mutant under ML, whereas photoprotection
260 factors (qE/NPQ) showed mixed patterns: *PSBS* transcripts were elevated in the mutant, but
261 *LHCSR* induction was attenuated relative to WT. In turn, *SPA1*, a component of the E3 ubiquitin
262 ligase complex (CUL4-DDB1-LRS1-SPA) involved in repression of PSBS- and LHCSR-mediated
263 qE (Gabilly et al., 2019; Aihara et al., 2019), was downregulated, implying altered control of qE
264 responses in *kea1*.
265 Because higher expression of protein quality control genes (*ClpP* and *FTSH*) was observed
266 in the plastid, we also analyzed markers of the chloroplast unfolded protein response (cpUPR).
267 Genes encoding cpUPR components—including *VIPP2* (sensing), *MARS1* (signaling), and
268 markers such as *CLPB3*, *DEG1C*, *FTSH2*, *HSP22E/F*, and *HSP70B* (Ramundo et al., 2014; Perlaza
269 et al., 2019; Theis et al., 2020)—were consistently upregulated in *kea1* compared to WT (Figure
270 4H), in most cases already at LL conditions i.e., 25 µE.

271 *Expression of ion transporters in kea1 is altered under low and moderate light*

272 When analyzing genes upregulated ($\log_2 FC \geq 1$) in *kea1* LL conditions, the GO term
273 potassium transport (GO:0006813) was significantly enriched (Supplemental Table S5). Within
274 this group, several HAK/KUP/KT-type high-affinity K^+ transporters (*HAK2*, *HAK4*) and
275 Na^+/SO_4^{2-} transporter-like genes (*SLT1-SLT3*) showed elevated transcript levels in the mutant
276 compared to WT (Figure 4I, Supplemental Figure S7F). These transporter families have previously
277 been linked to K^+ and sulfate acquisition and to the maintenance of cellular ion balance (Li et al.,
278 2023; Pootakham et al., 2010).
279 Inspection of the complete gene set within the potassium-transport category revealed that
280 expression changes persisted or became more pronounced under moderate light (ML). The same
281 transporters that were induced under LL remained among the most strongly upregulated genes

282 under ML, except *HAK2*, which decreased relative to WT. Additional transporters, including
283 *HAK3* and *NAK1*, the sole Na^+/K^+-ATPase-like pump homolog in Chlamydomonas, were also
284 induced. NAK1 and HAK-like proteins respond to low-potassium and saline stress and mediate
285 cytosolic K^+ and Na^+ homeostasis (Li et al., 2023). Hence, their upregulation in *kea1* suggests a
286 disturbance in cellular ion homeostasis and activation of low-potassium–responsive pathways,
287 possibly reflecting altered K^+ partitioning causing cytosolic potassium deficiency or impaired ion
288 signaling between the chloroplast and cytosol (Figure 4I).

289 Across the light-shift experiment, *SLT* and *HAK* family members, along with other
290 significant genes from this GO term, followed a similar trend in *kea1* (and partially in WT) in
291 response to the light treatment: transcript levels increased under ML and declined again during
292 recovery (RL), but transcription was consistently higher in the *kea1* mutant than in the WT
293 (Supplemental Figure S7F).

294 *KCN11*, a tonoplast K^+ channel required for osmoregulation, also showed significantly elevated
295 transcript levels ($\log_2FC = 0.43$) in *kea1* under ML (Figure 4I). The upregulation of KCN11 in
296 *kea1* thus supports the interpretation that loss of *CrKEA1* perturbs osmotic balance, consistent with
297 broader alterations in ion homeostasis.

298 In summary, loss of *CrKEA1* triggers a multifaceted transcriptional response pointing
299 towards a dual role for CrKEA1-dependent ion homeostasis in maintaining chloroplast translation
300 capacity and safeguarding protein folding.

301 *Species-Specific Consequences of KEA1 Loss for Plastid and Cell Cycle Regulation*

302 Having observed similar transcriptional upregulation of ribosome biogenesis genes in both
303 species upon *KEA* loss, we aimed to directly compare the broader transcriptomic responses
304 between Chlamydomonas and Arabidopsis IE *KEA* knockouts. To this end, we re-analyzed RNA-
305 seq data from Arabidopsis WT and *kea1kea2* mutants (DeTar et al., 2021; Supplemental Table S6)
306 and compared it with the RNA-seq data from the Chlamydomonas *kea1* mutant. To identify genes
307 commonly or uniquely regulated in response to IE *KEA1* disruption across species, we mapped
308 Chlamydomonas DEGs to their closest Arabidopsis homologs and categorized the results into
309 three groups: shared DEGs (genes differentially expressed in both species) and species-specific
310 DEGs (Supplemental Table S7).

311 GO term enrichment analyses on these categories (Figure 5A; Supplemental Table S8)
312 revealed that DEGs involved in ribosome biogenesis were largely shared between the two species,
313 indicating a conserved stress response linked to impaired rRNA maturation. In contrast, DEGs
314 related to the cell cycle were exclusively found in Chlamydomonas, suggesting a lineage-specific
315 consequence of *KEA1* loss on cell division control.

316 The Arabidopsis-specific DEGs were enriched for GO terms associated with, i.e.,
317 responses to various stimuli, including light, red and far-red light signaling, wounding, and
318 regulation of multicellular development—consistent with the plants' complex tissue architecture
319 and photomorphogenic signaling networks (Figure 5A).

320 A direct comparison at the level of DEGs further confirmed that ribosome biogenesis genes
321 are upregulated in both species (Figure 5B). However, cell cycle–related genes are strongly
322 downregulated in Chlamydomonas but not significantly altered in Arabidopsis. Interestingly, most
323 genes related to plastid fission showed opposite trends: they were downregulated (*MINE*, *MIND*,
324 *FTSZ1*, *ARC5*, *ARC6*) in Chlamydomonas but many slightly upregulated in Arabidopsis (*FTSZ1*,
325 *ARC6*, which are conserved in both) or not-significant (*MIND*). However, key plastid division
326 genes, like *PDV1* and *PDV2*, which are unique to land plants and determine plastid division rate
327 (Miyagishima et al., 2006; Okazaki et al., 2009, Holtsmark et al., 2013), and *MINE* and *ARC5*,
328 were slightly down-regulated in Arabidopsis.

329 *Plastid rRNA processing is impaired in both At and Cr kea1 mutants*

330 Given the transcriptional upregulation of ribosome biogenesis genes in both Arabidopsis
331 and Chlamydomonas IE *KEA* mutants (Figure 5B), we examined whether loss of *CrKEA1* in algae
332 also disrupts plastid rRNA maturation, leading to the accumulation of unprocessed rRNA
333 precursors as observed in plants (DeTar et al., 2021; DeTar et al., 2022). Notably, plastid rRNA
334 processing differs between the two lineages in several important aspects: 1) Arabidopsis generates
335 a 4.5S rRNA fragment from the 23S precursor, whereas Chlamydomonas instead produces the
336 distinct 7S and 3S fragments cleaved from the opposite end (Holloway and Herrin, 1998; Ahmed
337 et al., 2016; Schmid et al., 2024); 2) Chlorophytes employ much more octotricopeptide repeat
338 (OPR) RNA-binding proteins (RBP) while plants rely heavily on pentatricopeptide repeat (PPR)
339 proteins (Small et al., 2023). However, both systems rely on precise cleavage of large precursor

340 transcripts into functional ribosomal RNAs, which involves temporal sequence-specific RNA-
341 RBP interactions (Supplemental Figure S8).

342 To test for stromal rRNA maturation defects in Chlamydomonas, we analyzed total RNA
343 from *kea1* and WT cultures using rRNA sequencing. Initially, all stromal rRNA reads from *kea1*
344 and WT were aligned akin to previous studies (Hotto et al., 2015; Castandet et al., 2016). This
345 approach revealed increased read coverage within intergenic regions in *kea1*, particularly in the
346 7S and 3S regions derived from the 23S precursor. Since these fragments are removed during
347 rRNA maturation, their high abundance in *kea1* indicated mutant-specific accumulation of
348 unprocessed rRNA intermediates (Figure 6A, Supplemental Figure S9A, B). To corroborate these
349 observations, we carried out RNA blots employing stromal rRNA-specific probes. Indeed, a clear
350 accumulation of the 7S-3S-23S precursor was specifically observed in *kea1* cells (Figure 6B,
351 Supplemental Figure S10A, B). Splicing defects did not change with light shifts, but they were
352 less abundant in cells grown in TAP medium.

353 In summary, results from our RNA analyses suggest that despite significant differences in
354 rRNA structures and processing pathways between algae and land plants, the importance of IE
355 KEAs for seamless plastid rRNA processing is functionally conserved between chlorophytes and
356 streptophytes.

357 *Functional conservation of IE KEA transporters between algae and higher plants*

358 The rRNA processing phenotypes observed in plants and green algae suggest functional
359 conservation of IE KEAs across the green lineage. We therefore tested whether CrKEA1 can
360 substitute for its homologs AtKEA1/2 in Arabidopsis. Despite substantial amino acid sequence
361 divergence between CrKEA1 and AtKEA1, structural predictions generated with AlphaFold3
362 (DeepMind; Abramson et al., 2024) indicate a broadly conserved domain architecture (Figure 6C;
363 Supplemental Figure S11A-C; Gulati et al., 2024). Initially, we cloned full-length *CrKEA1* with a
364 C-terminal YFP. The finished construct *CrKEA1-YFP* was transformed into the *kea1-1kea2-1*
365 (hereafter simply *kea1kea2*) Arabidopsis mutant allele (Kunz et al., 2014). Several independent
366 transgenic *CrKEA1-YFP* lines exhibited robust complementation i.e., growth, leaf area, fresh
367 weight, and photosynthetic performance (F_v/F_m and ETR) were restored close to WT levels (Figure
368 6D; Supplemental Figure S12). Subsequent immunoblotting confirmed the accumulation of
369 CrKEA1-YFP in the transgenic lines at the expected apparent size of ~140 kDa (Figure 6E).

370 Next, we conducted RNA blots with WT, *kea1kea2*, and *CrKEA1-YFP* complemented lines
371 and found that CrKEA1-YFP restores plastid 23S rRNA processing (Figure 6F).
372 Together, these findings demonstrate that despite a billion years of divergence, CrKEA1
373 retains sufficient functional similarity to AtKEA1/2, which reveals a strong evolutionary
374 conservation of K^+/H^+–mediated effects on ribosome biogenesis. Curiously, when expressed in
375 Arabidopsis, CrKEA1-YFP localized in discrete, rod-like structures, whereas the endogenous
376 AtKEA1-YFP appeared in discrete spots (Figure 6G).

377 *Comparison of co-expression networks reveals a divergent cell cycle embedding in Arabidopsis*
378 *and Chlamydomonas*

379 Since the GO terms *cell cycle* and *plastid fission* were affected in the Chlamydomonas
380 mutant but not in Arabidopsis, we carried out an in-depth comparison between the respective co-
381 expression networks (Figure 7A). Direct co-expression involves "*gene to gene*" interactions, while
382 secondary co-expression involves "*gene to intermediary gene to gene*" interactions. In the
383 Chlamydomonas co-expression network (ML condition based), *ARC5*, *ARC6*, and *MIND,* all
384 scoring a $\log_2$FC < -2, were found to be secondary neighbors in a shared cluster with cell cycle
385 genes: e.g., *MIND* with the key *cell cycle* gene *CDKB1(2)* but also *ARC5* with *TOPII*, *TPX2*,
386 *AUR2*, *MCM5*, *WEE1* that were similarly downregulated with a $\log_2$FC < -1. This indicates that
387 both biological processes have tightly co-expressed interactions resulting in unidirectional
388 expression changes.
389 Interestingly, in Arabidopsis co-expression networks, *cell cycle* genes show little to no
390 regulatory concordance with *plastid fission* genes. Transcripts of *ARC5*, *PDV1*, and *PDV2*
391 displayed $\log_2$FC values between -0.75 and 0, while *FTSZ2-1*, *FTSZ2-2*, *ARC6*, *MSL2*, *MSL3*,
392 *MCD1*, *KASI*, *MURE*, and *AT2G21280* (*GC1*) ranged between 0 and 0.75, indicating that
393 regulating these genes in response to the loss of IE *KEA* had little biological significance for
394 Arabidopsis. While certain genes involved in Arabidopsis chloroplast division were regulated with
395 absolute values higher than a $|\log_2\text{FC}|$ of 0.75 (ie. upregulated *YLMG1-1* and *FTSHi1*), they were
396 not concertedly downregulated with *cell cycle* genes as in Chlamydomonas.
397 To further substantiate co-expression between *cell cycle* and *plastid fission* genes, we
398 plotted the percentage of co-expressed interactions (direct and secondary) for each species (Figure
399 7B). Within the Arabidopsis co-expression network, 5.3% (4 genes) are direct interactors, while

400 94.7% (72 genes) are secondary interactors. However, none of these genes were strongly
401 ($|\log_2 FC| \geq 0.75$) differentially expressed in *kea1kea2* mutants. For Chlamydomonas, 100% (4
402 genes) of the genes are involved in secondary interactions, with 75% (*ARC5*, *ARC6, MIND*)
403 showing co-regulated downregulation.

404 To identify orthologs of *cell cycle* genes in Chlamydomonas and Arabidopsis, we used an
405 orthogonal approach building on CoNekT (Figure 7C). When comparing co-expression clusters of
406 TOPII, we found several *cell cycle* genes were orthologs between species. *ROW1*, *MCM10*,
407 *PAKRP1L*, *POK1*, *POK2*, *ZCF125* were found to have orthologs within Chlamydomonas that were
408 not annotated by best BLAST hits. Within this gene family, three Chlamydomonas genes were
409 grouped together with seven genes. For *plastid fission* genes, no apparent similarity between
410 Chlamydomonas and Arabidopsis clusters were found. This analysis also indicates that the
411 biological process *cell cycle* in Chlamydomonas showed certain similarities with Arabidopsis.

412 *Single-Cell Time-Lapse Imaging Reveals Cell Cycle irregularities in kea1*

413 *kea1* mutant cells displayed pronounced size distribution differences in micrographs and
414 when analyzed by flow cytometry (Figure 3D). In addition, coordinated downregulation of cell
415 cycle and chloroplast division genes was observed in the *kea1* transcriptome (Figure 4D, E). In
416 Chlamydomonas, cell division proceeds via a multiple fission cycle, in which cells undergo n
417 divisions (S/M phase) into 2^n daughter cells after a prolonged G1 phase. The size of the mother
418 cell determines the number of divisions resulting in 2, 4, 8, 16, etc. equally sized daughter cells
419 (Figure 8A; Cross and Umen, 2015).

420 The intrinsic heterogeneity of batch cultures poses substantial challenges for the
421 identification of cell cycle stage-specific defects. To overcome these limitations, we developed a
422 live-imaging platform capable of tracking individual cells over several days. Cells were applied to
423 a custom-made, biologically inert hydrogel with multiple chambers embedded in a flow cell chip
424 (Figure 8B). Our design allows for tight temperature- and light-control, constant medium flow,
425 nutrient diffusion, and continuous imaging throughout Chlamydomonas cell division cycles. In
426 addition, the multiple chambers situated on a single chip enabled simultaneous side-by-side growth
427 and monitoring of WT and *kea1* mutant strains under the exact same controlled culturing
428 conditions in TAP medium at 25 µE (Figure 1G).

429 WT cells displayed regular and symmetric division with high fidelity, verifying ideal and
430 well-suited growth conditions in our continuous flow cell chip setup (Figure 8C; Supplemental
431 Figure S13A). By contrast, our analysis revealed several key differences in the mutant compared
432 to WT: *kea1* cells were significantly larger than WT cells during every segment of the G1-division
433 cycle (Figure 8D). Interestingly, the elevated volume of *kea1* cells can be traced back to the mid-
434 G1 phase (Supplemental Figure S13B), when mutant cells exhibit a significantly higher volume
435 increase than WT. Additionally, mutant cells not only remained longer in the G1 phase (Figure
436 8E) but also took longer to complete the S/M phase (Figure 8F).
437 Upon closer examination, specific cytokinesis defects were observed more frequently in
438 *kea1* mutants: 1) Divisions often produced daughter cells of unequal size (Figure 8G), hinting at a
439 misplaced division plane. Further analysis of mutant daughter cells revealed that these birth
440 volume deviations did not affect subsequent G1-division cycle length differences compared to
441 those of WT daughters (Supplemental Figure S13C). 2) Re-merging of seemingly already divided
442 cells multiple hours into the G1 phase was observed in approximately 3% of all *kea1* divisions but
443 was never detected in WT (Figure 8H). Remerged cells divided into 3 or 5 daughter cells after
444 completing their G1 phase (Supplemental Figure S13A), possibly due to two coexisting nuclei in
445 a single remerged cell.
446 Our single-cell imaging revealed pronounced defects in cell cycle progression and division
447 fidelity, confirming the transcriptomic observations.

448 **Discussion**

449 Plastid integrity relies on tightly controlled ion fluxes across the inner envelope membrane.
450 Our findings establish CrKEA1 as the functional counterpart of AtKEA1/2 in Arabidopsis, adding
451 experimental evidence to the hypothesis that KEA function in the envelope must have been
452 established very early in the evolutionary history of plastids i.e., the endosymbiotic event. Loss of
453 *CrKEA1* impairs plastid structure, photosynthesis, ribosome biogenesis, and cell cycle regulation
454 in Chlamydomonas, revealing both deep conservation and lineage-specific divergence in KEA
455 function across the green lineage (Figure 9).
456 In Arabidopsis, disruption of *AtKEA1/2* causes increased cellular potassium levels, fragile
457 chloroplasts, impaired photosynthesis, and growth (Kunz et al., 2014; Aranda-Sicilia et al., 2016).
458 We observed similar defects in *kea1* mutants, including altered ion balance, growth delay,

459 spherical plastids lacking the characteristic cup shape, and reduced photosynthetic efficiency.
460 These parallels indicate that KEA activity at the plastid envelope might be broadly required for
461 maintaining the ion homeostasis necessary for plastid ultrastructure and function. The strong
462 conservation of this role was underscored by cross-species complementation, in which CrKEA1
463 restored growth, photosynthesis, and rRNA processing in Arabidopsis *kea1kea2* mutants. This
464 accentuates the potentially fundamental role of IE KEAs in supporting cellular biochemistry by
465 maintaining pH and ion homeostasis in phototropic eukaryotes — a function that may have been
466 conserved since the last common ancestor, likely persisting through more than a billion years of
467 evolutionary divergence (for molecular clock, see Strassert et al., 2021 and Bierenbroodspot et al.,
468 2025).

469 Consistent with this deep evolutionary conservation are the parallels between plants and
470 algae in the role of KEA transporters in plastid rRNA maturation. In Arabidopsis, loss of
471 AtKEA1/2 disrupts rRNA processing and plastid translation (DeTar et al., 2021). Similarly,
472 Chlamydomoans *kea1* mutants accumulated unprocessed 23S-derived precursors, in accordance
473 with impaired maturation. Although the 23S rRNA maturation pathways differ between algae and
474 plants — Chlamydomonas generates unique 7S and 3S fragments, whereas Arabidopsis produces
475 a separate 4.5S rRNA from the opposite end of the 23S precursor — the accumulation of immature
476 rRNA in Chlamydomonas *kea1* closely mirrors the maturation defects seen in Arabidopsis
477 *kea1kea2* (DeTar et al., 2021; DeTar et al., 2022). Structural work offers a mechanistic basis for
478 this observation, showing that potassium and magnesium ions are required to stabilize rRNA and
479 the large ribosomal subunit (Nierhaus, 2014; Rozov et al., 2019; Klein et al., 2004). Ion imbalance
480 in *kea1* mutants could therefore destabilize rRNA precursors and interfere with their proper
481 processing, or indirectly affect maturation through feedback on ribosome assembly (DeTar et al.,
482 2021). Together, our findings strengthen the model that ion imbalance destabilizes rRNA
483 secondary structures and disrupts ribosome biogenesis across systems, despite lineage-specific
484 differences in processing outcomes.

485 Transcriptomic profiling revealed a conserved upregulation of ribosome biogenesis genes
486 and downregulation of PhANGs in *kea1*, mirroring the Arabidopsis *kea1kea2* response (DeTar et
487 al., 2021). In both species, repression of photosynthetic gene expression likely reflects a protective
488 adjustment to plastid dysfunction. In Arabidopsis *kea1kea2* mutants, the retrograde response is a
489 GUN1-mediated GOLDEN2-LIKE (GLK1/GLK2) transcription factor suppression to delay

490 chloroplast biogenesis, thereby minimizing photo-oxidative damage until stress has been resolved
491 (DeTar et al., 2021; Richter et al., 2023). However, this regulatory logic is unlikely to apply to
492 Chlamydomonas: 1) GLK1/2 emerged as a hub controlling the genetic networks that underpin
493 chloroplast differentiation and photomorphogenesis only in zygnematophytes (Dadras et al.,
494 2023), and 2) although GUN1 is evolutionarily ancient, its role in retrograde signaling is thought
495 to have arisen after streptophyte algae diverged from chlorophytes (Honkanen and Small, 2022).
496 Thus, PhANG suppression in Chlamydomonas must rely on different upstream cues. In *kea1*,
497 where we also found induced ROS-responsive transcripts, an upregulation of *PCYA*, a bilin-
498 synthesis gene, points to tetrapyrrole-derived retrograde signals to repress PhANGs during plastid
499 stress as a coping mechanism (Duanmu et al., 2013).

500 The concurrent induction of Na^+/SO_4^{2-} (SLT1–3;Pootakham et al.,2010) and K^+
501 transporters (particularly *HAK*, *NAK;* Li et al., 2023) together with the altered expression of other
502 ion pumps, exchangers and channels, indicates that the ionic imbalance in Chlamydomonas *kea1*
503 extends beyond chloroplast potassium homeostasis. These regulatory patterns may reflect systemic
504 compensatory responses to altered ion gradients or membrane potentials resulting from impaired
505 K^+/H^+ exchange at the plastid envelope. Increased sulfate uptake could further support glutathione
506 biosynthesis, mitigating oxidative stress associated with disturbed ion balance (Niyogi, 1999;
507 Zhang et al., 2004). Also, the tonoplast K^+ channel *KCN11* was slightly upregulated. Interestingly,
508 *kcn11* mutants display growth defects under nitrogen limitation, including enlarged cell size (Xu
509 and Pan, 2020; Fauser et al., 2022; Vilarrasa-Blasi et al., 2024). These findings point towards the
510 functional coupling of potassium and sulfate fluxes as part of the wider physiological
511 consequences of disrupted KEA-mediated ion transport in Chlamydomonas. In addition to these
512 conserved features, IE *KEA* loss in Chlamydomonas exhibited lineage-specific consequences. *kea1*
513 mutants showed constitutive induction of the MARS1-dependent chloroplast unfolded protein
514 response (cpUPR; Perlaza et al., 2019). Unlike Arabidopsis, where cpUPR markers were absent
515 or even downregulated (e.g., *CLPB3*) in *kea1kea2* (DeTar et al., 2021), Chlamydomonas activates
516 these stress pathways constitutively (already under low light), indicating destabilized stromal
517 protein homeostasis as soon as ion balance is disrupted by loss of *CrKEA1*. This points to a lineage-
518 specific strategy: whereas multicellular plants can attenuate plastid protein synthesis and postpone
519 chloroplast biogenesis to avoid protein aggregation, the single-celled alga Chlamydomonas cannot

520 completely postpone chloroplast function without jeopardizing survival. Thus, the unicellular alga
521 must maintain translation in its single essential plastid and instead relies on cpUPR pathways to
522 counteract misfolding and aggregation (Dogra et al., 2019; Perlaza et al., 2019; Richter et al.,
523 2023).

524 Further characteristic observed in Chlamydomonas *kea1* mutants were enlarged cells, an
525 extended G1 phase, irregular cytokinesis, and strong downregulation of cell division genes. Both
526 *CDKB1* and its partnering cyclins (*CYCA1*, *CYCB1*) were strongly downregulated, consistent with
527 defects in mitotic progression and multiple fission cycles (Tulin and Cross, 2014; Bisova et al.,
528 2005). The partial reduction of D-type cyclins further weakens G1/S entry, while the mild
529 repression of CDKG1 implicates misregulation of size-dependent checkpoints (Li et al., 2016;
530 Umen and Goodenough, 2001). The coupled downregulation of plastid fission genes that we found
531 through co-expression network analyses aligns with the tight synchronization between plastid
532 division and cell cycle progression in unicellular algae (Sumiya et al., 2016; Clark-Cotton et al.,
533 2025). It was shown that conditional repression of plastid genes (*rpoA*, *rps12*) that are required for
534 the expression machinery halts Chlamydomonas growth whereas cells resume proliferation once
535 chloroplast function is restored (Ramundo et al., 2013). The cell cycle in *kea1* is not arrested.
536 Mutant cells only progress through G1 more slowly and delay cell and chloroplast division, but
537 the perfect coordination between plastid and cell cycle remains defective. As a result, division
538 errors occur at an increased rate, especially when shifted to elevated light intensity, an inherent
539 trigger for algae to accelerate growth and the rate of division (Dupuis et al., 2025).
540 In contrast to the single plastid in Chlamydomonas, plant plastids divide autonomously,
541 controlled by developmental programs, tissue context, and land-plant-specific proteins such as
542 PDV1/2 (Okazaki et al., 2009; Vercruyssen et al., 2015). Thus, while IE *KEA* loss in both systems
543 impairs plastid function, the downstream impact is filtered through fundamentally different
544 organizational logics: plastid–cell cycle coupling in algae versus tissue-specific developmental
545 regulation in plants. However, our finding that *kea1* cells downregulate plastid division and
546 consequently accumulate enlarged chloroplasts parallels observations in Arabidopsis, where
547 *kea1kea2* mutants harbor fewer but enlarged plastids per cell (Kunz et al., 2014; Aranda-Sicilia et
548 al., 2016). Despite differences in cellular architecture — one plastid per algal cell versus many

549 plastids per plant cell — KEA transporters thus appear broadly required to coordinate plastid
550 division and maintain organelle size.

551 **Conclusions**

552 Given that potassium fluxes have universal roles in driving cell-cycle progression in
553 microalgae and beyond (Urrego et al., 2014; Feeney et al., 2016; Henslee et al., 2017; Rodríguez
554 et al., 2024), our integrated ionomics-single-cell imaging approach offers a roadmap for future
555 studies to unravel how perturbations in organellar ion transport translate into systemic defects in
556 growth, proliferation, and stress adaptation. Taken together, our results demonstrate that IE KEA
557 transporters are evolutionarily conserved regulators of plastid homeostasis, linking ion transport
558 to ribosome assembly and photosynthetic capacity. Yet the downstream phenotypes diverge,
559 reflecting the distinct cellular architectures of unicellular algae and multicellular plants. *kea1*
560 mutants expose defects in cell cycle fidelity absent in plants, while Arabidopsis mutants reveal
561 developmental and signaling adjustments not observed in algae. These findings illuminate how
562 plastid ion transport serves as a deeply conserved module, whose consequences for cell physiology
563 depend on lineage-specific evolutionary trajectories.

564 **Material and Methods**

565 *Algae cultivation and growth measurements*

566 All Chlamydomonas (*Chlamydomonas reinhardtii*) *kea1* mutants and complementation lines
567 generated in this study share the CC-406 cw15 mt- background (Davies and Lyall, 1973) which
568 served as the reference ("wild type", WT) in this study.

569 Algae were grown in Tris-acetate-phosphate (TAP; Gorman and Levine, 1965) medium under
570 constant light of 25 µmol photons m^{-2} s^{-1} at 23°C and shaking at 125 rpm if in liquid culture, unless
571 indicated otherwise. TAP was supplemented with 1% (w/v) sorbitol for culturing strain cc406. For
572 photoautotrophic conditions algae were grown in Sueoka's high salt medium (HSM; Sueoka,
573 1960).

574 The optical density at 750 nm (OD750) of liquid cultures was determined by a UV-vis
575 spectrophotometer and the cell count ml^{-1} by a BD Accuri™ C6 plus flow cytometer. To determine
576 a conversion factor to calculate the size of the cells measured from FSC-A, the flow cytometer was

577 calibrated with CS&T RUO Beads (BD Biosciences, USA). The derived linear regression was y =
578 2.432 x10^6 x + 1,706 with y being the diameter (µm) and x the FSC-A values.

579 *Plant growth and generation of CrKEA1-YFP plants*

580 Arabidopsis (*Arabidopsis thaliana*) plants were grown at 110 µE illumination in long-day
581 conditions (16 h/8 h at 22°C). To generate transgenic *CrKEA1* Arabidopsis plants, the codon-
582 optimized *CrKEA1* coding sequence (Cre04.g220200_4532.1, fused to a Twin-Strep tag) was
583 cloned into the binary Ti vector *pG20_TEV_mVenus_Hyg* via Golden Gate assembly downstream
584 of the UBQ10 promoter (Addgene ID #240651; Schwartz et al., 2025) as described in
585 Supplemental Table S9. Venus is referred to throughout as YFP. The resulting *CrKEA1-*
586 *TwinStrep-TEV-YFP* (short *CrKEA1-YFP*) fusion construct was used for stable transformation of
587 the Arabidopsis T-DNA insertion line *kea1-1kea2-1* (Kunz et al., 2014). The final construct was
588 transformed into Arabidopsis via the *Agrobacterium tumefaciens* (GV3101 containing *pSOUP*) by
589 the floral dip method as described previously (Clough and Bent, 1998). The T1 generation was
590 selected on 25 µg/ml Hygromycin-containing 1/2 strength MS medium (Murashige and Skoog,
591 1962) and screened for phenotypical rescue of the *kea1-1kea2-1* mutant. Expression of *CrKEA1-*
592 *YFP* was verified via immunoblotting (Höhner et al., 2019).

593 *Generation of Chlamydomonas kea1 mutants by CRISPR/Cas9*

594 *kea1* mutants were created in CC-406 cw15 mt^- using insertional mutagenesis by the
595 CRISPR/Cas9 technique following the protocol established (Greiner et al., 2017). Briefly, a
596 crRNA sequence was designed to target *CrKEA1* exon-19. The crRNA was annealed with
597 tracrRNA (Integrated DNA Technologies, #1072533) to generate guide RNAs (gRNA) and then
598 conjugated with Alt-R® S.p. Cas9 Nuclease V3 (Integrated DNA Technologies, #1081058) to
599 form the SpCas9/gRNA complex. The latter was co-transformed into Chlamydomonas with a
600 mutation oligonucleotide containing orientation and frameshift tolerant STOP codons and with the
601 plasmid pBC1 (pJR38, Neupert et al., 2009) conferring paromomycin resistance. Transformation
602 was carried out on a NEPA21 electroporator (Nepa Gene). Cells were selected under 10 µg ml^{-1}
603 paromomycin and screened by colony-PCR. Knock-out of *CrKEA1* was confirmed by
604 immunoblotting using CrKEA1 antibodies. Relevant sequences are listed in Supplemental Table
605 S1.

606 *Generation of kea1 complementation lines*

607 The *CrKEA1* gDNA sequence, including the native promoter, was inserted into *pLM161* (Cr-
608 Venus-3xFLAG; hygromycin), applying the recombineering approach described in Emrich-Mills
609 et al., 2021; Supplemental Table S10). Nuclear transformation was achieved by the glass bead
610 method (Kindle, 1990). Transformed *kea1* cells were selected under 100 µg ml^{-1} hygromycin
611 followed by screening for the expression of the CrKEA1-YFP fusion protein by fluorescence
612 microscopy and immunoblot.

613 *Design of the CrKEA1 antibody*

614 To generate antibodies against CrKEA1, a DNA fragment codon optimized for *E. coli* synthesized
615 by Twist Bioscience (California, USA), was cloned into the plasmid *pHue* (Catanzariti et al., 2004;
616 modified for Gold Gate cloning) resulting in the plasmid *pHue_CrKEA1-aa94-337* (Supplemental
617 Table S11). Proteins were expressed in *E. coli* strain BL21 (DE3) overnight at 23°C and lysed in
618 lysis buffer (20 mM Tris-HCl, pH 8.0, 300 mM NaCl and 10 mM imidazole). The HisUbiquitin-
619 tagged CrKEA1 fragment was extracted by an IMAC column, the tag was cleaved by Ubiquitin
620 Specific Peptidase 2 (USP2; Baker et al., 2005) and the sample passed over a size exclusion
621 chromatography (SEC) column in SEC buffer (20 mM Tris-HCl, 300 mM NaCl). The SEC elution
622 was reapplied to an IMAC column, where the tag-less protein was recovered from the flow-
623 through. The pure protein CrKEA1-aa94-337 in 20 mM Tris pH 8, 200 mM NaCl, and 5% glycerol
624 served BioGenes (Berlin, Germany) as antigen to produce polyclonal antibodies. Serum was used
625 for immunodetection.

626 *Protein extraction and immunoblotting*

627 For Chlamydomonas, cultures grown to an OD750 of 2 were pelleted and resuspended in Laemmli
628 SDS loading dye containing 50 mM DTT. Samples set to an OD of 22 were heated to 60°C for 20
629 min and then subjected to SDS PAGE. Immunoblotting was performed on PVDF membranes with
630 secondary antibodies coupled to horse radish peroxidase and the enhanced chemiluminescence
631 (ECL) system. For Arabidopsis, immunoblotting was performed as described before (Höhner et
632 al., 2019). The following antibodies were used: GFP (Roche 11814460001), NAB1 (Agrisera
633 AS08 333), AtKEA1 (Bölter et al., 2020), CrKEA1 (this study)

634 *Element determination via TXRF*

635 Cultures for element analysis were washed thrice in isotonic buffer (300 mM sorbitol, 20 mM
636 HEPES pH 7.5, 5 mM EDTA, 10 mM $NaHCO_3$). Cell numbers in washed samples were
637 individually determined for each sample using a Neubauer Improved counting chamber (Hecht-
638 Assistent, Sondheim vor der Rhön, Germany). Elemental analysis was performed by total
639 reflection X-ray fluorescence (TXRF) using an S4 T-STAR (Bruker, Berlin, Germany) as
640 described in Holzner et al., 2025. The sample was mixed in a 1:1 ratio with internal standards to
641 final concentrations of 1 ppm vanadium (W-L) and 1 ppm gallium (Mo-K) and 0.1% (w/v)
642 polyvinyl alcohol (PVA). Samples were applied to silicon-coated quartz glass carriers and
643 measured at 50 kV for 1000 s per sample using Mo-K and W-L excitation. Element concentrations
644 were normalized to the cell number of each sample. To determine background element levels, a
645 sample of isotonic buffer was measured, which was subtracted from the respective samples.

646

647 *Pulse-Amplitude-Modulation (PAM) fluorometry and leaf area*

648 The IMAGING-PAM (M-Series Maxi, Walz GmbH, Effeltrich, Germany) was used for leaf area
649 and PAM measurements. For Arabidopsis, experiments were performed as described previously
650 (Schneider et al., 2019). For Chlamydomonas drop cultures, spotted cultures were cultivated under
651 standard conditions for 3 days before subjecting them to PAM measurements. For liquid culture,
652 cells grown in 50 ml were adjusted to an OD of 1.5, and equal volumes (2 ml) were transferred
653 into multi-well plates for PAM measurements after 15 min dark adaptation.

654 *Localization of CrKEA1-YFP in algae with fluorescence microscopy*

655 Chlamydomonas cells expressing CrKEA1-YFP were imaged with the DMi8 Inverse Fluorescence
656 Thunder Microscope (Leica, Wetzlar). For chlorophyll autofluorescence, cells were illuminated
657 for excitation with 440 nm and position 642/80 of the emission filter cube CYR-LED8 was chosen
658 for detection. For YFP signals, excitation was set to 510 nm and cube position to 535/70.

659 *Protoplasts isolation and localization of CrKEA1-YFP in Arabidopsis by fluorescence microscopy*

660 Protoplasts were isolated from Arabidopsis leaves as described before (Wu et al., 2009).
661 Visualization was carried out using a Stellaris 5 confocal laser scanning microscope (Leica,
662 Wetzlar). Chlorophyll was excited using a diode 408 nm laser and detected with detector HyD

663 between 620 and 810 nm, while YFP was excited using the WLL laser set to 515 nm and detected
664 with HyD between 520 and 580 nm.

665 *Transmission Electron Microscopy*

666 Sample preparation was performed as previously described (Lübben et al., 2024). Chlamydomonas
667 samples were frozen under high pressure (2,100 bar) in culture medium using an EM HPM100
668 (Leica Microsystems, Germany). Following cryofixation, samples underwent freeze substitution
669 (Peschke et al., 2013; Walther and Ziegler, 2002) in an EM AFS2 system (Leica Microsystems),
670 after which they were embedded in Epon 812 and polymerized for 16 h at 63 °C. Ultrathin sections
671 of 50 nm (ultra 35°, 3.0 mm, DiATOME) were cut on an Ultracut E ultramicrotome (Leica
672 Microsystems) and collected on collodion-coated, 400-mesh copper grids (Science Services
673 GmbH, Germany). Prior to imaging, sections were post-stained with lead citrate (Reynolds, 1963).
674 Samples were examined in a Zeiss EM 912 transmission electron microscope (Zeiss, Germany)
675 equipped with an integrated OMEGA energy filter operated in zero-loss mode at 80 kV. Images
676 were captured at a nominal magnification of 12,500× using a 2k×2k slow-scan CCD camera
677 (Tröndle Restlichtverstärkersystem, Germany).

678 *Whole Genome Sequencing*

679 gDNA was isolated according to Dutcher et al., 2012 and sent to BMKGene (Biomarker
680 Technologies, Münster, Germany / Hongkong) for Illumina sequencing. CLC Genomics
681 Workbench and Integrative Genomics Viewer (IGV) was used to confirm stop codon insertion in
682 exon 19. TDNAscan (Sun et al., 2019) was used to search for additional off-target insertions.

683 *RNA-seq after ribo-depletion, Gene Ontology analysis, and constructing co-expression networks*

684 Four replicates per genotype and condition were sampled to obtain RNA-seq from the light shift
685 experiment. RNA was extracted using TRIzol™ reagent (Ambion, USA; Simms et al., 1993)
686 following the manufacturer's instructions. RNA was further purified and DNA contaminations
687 were removed using the Monarch® RNA Cleanup Kit (NEB) according to the manufacturer's
688 protocol. RNA quality control, depletion of ribosomal RNA, library preparation, and eukaryotic
689 lncRNA Sequencing was performed by BMKGene on an Illumina platform, generating over 10
690 Mio paired-end reads (150 bp) per sample. RNA-seq data were analyzed on the Galaxy platform
691 (usegalaxy.eu; Galaxy-Community, 2024) using the tools, reference genome and annotation file

692 (JGI Phytozome) listed in Supplemental Table S12. For statistical analysis and assessment of
693 differentially expressed genes (DEGs), the low read count filters were set to "1-count-per-million"
694 (CPM=1) in at least 3 samples. DEGs were considered significant with an adjusted p-value < 0.05.
695 Gene Ontology (GO) term enrichment was assessed with g:Profiler (Kolberg et al., 2023) and
696 condensed with REVIGO (Supek et al., 2011). Co-expression networks were calculated using the
697 StreptoNet (https://rshiny.gwdg.de/apps/streptonet/) framework (Dadras et al., 2023) and
698 constructed based on gene lists of interest. Chlamydomonas genes were annotated using the best
699 BLAST hits against Arabidopsis genes. CoNekT (https://conekt.sbs.ntu.edu.sg/) framework was
700 used to compare clusters of co-expression networks. See Supplemental Table S12 for further
701 details.

702 *RNAseq with focus on ribosomal RNA (MiSeq NGS)*

703 To analyze plastid rRNA processing, RNA was extracted from cells grown in HSM under
704 moderate light (100 µmol m^{-2} s^{-1}) as mentioned above. Library preparation was performed using
705 the NEBNext® Ultra™ II RNA Library Prep Kit (NEB). RNA and library quality were assessed
706 using the Agilent 2100 Bioanalyzer. Next-generation sequencing (2 × 300 paired-end) was carried
707 out on a MiSeq sequencer (Illumina, San Diego, CA, USA), generating over 1.5 million paired-
708 end reads per sample with a length of 200-250 nt. Data processing was performed on usegalaxy.eu
709 (Galaxy-Community, 2024) as described above. The effective genome size (113,516,734 bp) was
710 determined by subtracting the total number of ambiguous (N) bases (1,114,981 bp) from the actual
711 Chlamydomonas genome size (114,631,715 bp). To analyze coverage differences between
712 samples, mapped reads were processed through the BamCoverage and BamCompare pipelines of
713 the deepTools suite (Ramírez et al., 2016), focusing on plastome rRNA transcripts. BigWig output
714 files generated from both tools were exported as bedGraph (.csv format).

715 *Non-Radioactive RNA blots*

716 RNA blots were performed using 3'-Digoxigenin (DIG)-labeled DNA probes from metabion
717 international AG, Germany (Supplemental Table S13; Holtke & Kessler 1990; Ramkissoon et al.,
718 2006). RNA samples were denatured at 55°C for 45 minutes in denaturing buffer (15% (v/v)
719 DMSO, 7% (w/v) Glyoxal in 20 mM MOPS, 5 mM sodium acetate, 1 mM EDTA, pH 7) before
720 adding loading dye. Samples were separated on a 1.2% agarose MOPS gel at 4°C, and transferred
721 onto a nylon membrane via capillary blotting in 20x SSC (3M NaCl, 0.3M Trisodium Citrate

722 dihydrate, pH 7) overnight, followed by UV crosslinking. To develop the blot, the DIG Northern
723 Starter Kit (Roche, Cat. No. 12 039 672 910) was utilized as described by the manufacturer but
724 using 50°C for hybridisation.

725 *Single-cell time-lapse imaging and image analysis*

726 The microchannel layout was based on the original *Mother Machine* design for bacterial single-
727 cell studies (Wang et al., 2010) and was modified to enable the observation of Chlamydomonas
728 under hydrogel-mediated confinement. Hydrogel patterning was carried out using the
729 photolithographic microfabrication workflow previously described for PEG-based hydrogels
730 (Stöberl et al., 2023), with adjustments to the precursor composition and pattern geometry. Flow
731 channels were filled with diluted cultures (5×10^4 cells mL^{-1}) and placed in a stage-top chamber
732 (okolab, H101-CRYO-BL) connected to a cryostatic water bath (Lauda, RE415S). The medium
733 temperature was adjusted to 23°C and flow rate to 200 µl h^{-1}. Cells were continuously illuminated
734 with 25 µE. Images were acquired every 5 min on a Leica DMi8 Thunder microscope (Leica,
735 Wetzlar) using LASX. Chlorophyll autofluorescence was excited with a Leica LED8 at 475 nm
736 and detected with a Leica DFC9000 GTC camera with a 642/80 filter. Image analysis was
737 conducted in Cell-ACDC (Padovani et al., 2022). A custom-trained Cellpose (Pachitariu and
738 Stringer, 2022) model was used to segment cells. Segmentation was controlled and corrected in
739 the Cell-ACDC GUI. Segmented objects were then tracked with Trackastra (Gallusser and
740 Weigert, 2025) with the general_2d model using the chlorophyll autofluorescence channel as
741 input. Truthful tracking was checked in the Cell-ACDC GUI. Out-of-focus cells, division failures
742 and cells with an unobservable future were manually marked in the Cell-ACDC GUI for filtering
743 in downstream analysis. Resulting .csv files were filtered and analysed in a custom phyton script.

744 *Sequence alignment, structure prediction, and domain annotations*

745 Multiple Sequence alignment was performed by the *MultAlin* online tool (Corpet 1988). Structural
746 models were predicted using AlphaFold3 (DeepMind; Abramson et al., 2024). The default
747 parameters were used, and no experimental structural constraints were applied. For model
748 visualization, we used UCSF ChimeraX (Pettersen et al., 2021). For domain annotations,
749 information obtained from Uniprot.org (Q9ZTZ7) and AlphaFold3 prediction was combined.

750 *Accession numbers and annotations*

751 Chlamydomonas strains CC-406 cw15 mt$^-$, CC-4533 cw15 mt$^-$, the CLiP line (Li et al., 2016)
752 LMJ.RY0402.187220, and the BAC (well number 19-B-5) encoding the *CrKEA1*
753 (Cre04.g220200_4532.1) gDNA were obtained from the Chlamydomonas Resource Center
754 (University of Minnesota, USA). The Arabidopsis T-DNA insertion mutant *kea1-1kea2-1*
755 (SAIL_586_D02, SALK_045324) (Kunz et al., 2014) is available in the stock centers: ABRC:
756 CS72318 or NASC: N72318. All other GeneIDs are listed in the Supplemental Table S14 and S15.
757 RNA-seq data generated in this study have been deposited in the NCBI Sequence Read Archive
758 (SRA) under BioProject accession number PRJNA1343327 (Wunder et al., 2025)

759 **Supplemental Data**

760 Supplemental Figure S1: Figure S1: Alignment of inner envelope (IE) KEA protein sequences
761 from Chlamydomonas and Arabidopsis.
762
763 Supplemental Figure S2: Figure S2: Generation of the CrKEA1 antibody and testing the CLiP line.
764
765 Supplemental Figure S3: Figure S3: Genomic characterization of the kea1 CRISPR/Cas9 knock-
766 out site and immunoblotting.
767
768 Supplemental Figure S4: Figure S4: Genomic characterization of the *kea1* CRISPR/Cas9 knock-
769 out site (part2).
770
771 Supplemental Figure S5: Figure S5: Characterization of the *kea1* mutant and *CrKEA1-YFP*
772 complementation lines.
773
774 Supplemental Figure S6: Figure S6: Scatter plots corresponding to the flow cytometry experiment
775 shown in Figure 2.
776
777 Supplemental Figure S7: Figure S7: Additional results related to the RNA-seq experiment.
778
779 Supplemental Figure S8: Figure S8: Comparison of plastid rRNA processing pathways in
780 Chlamydomonas and Arabidopsis.
781
782 Supplemental Figure S9: Figure S9: rRNA-seq analysis of plastid rRNA processing including the
783 *CrKEA1-YFP* complementation line.
784
785 Figure S10: RNA blot analysis of plastid rRNA processing in the *kea1* mutant.
786
787 Figure S11: Structural comparison of AtKEA1 and CrKEA1.
788
789 Figure S12: Characterization of the Arabidopsis *kea1kea2* line complemented with *CrKEA1-YFP*.
790
791 Figure S13: Single cell live imaging of *kea1* and WT.
792
793 Supplemental Tables
794
795 Supplemental References

Acknowledgements

At LMU, we thank Berina Isakovic and Yuling Ma for help in isolating *kea1* mutant and complementation lines, Andreas Brachmann for supervising the rRNA seq experiment, and Nikolay Kayo Manavski and Jörg Meurer for teaching RNA work, Stefan Stöberl and Bettina Bölter for discussions about hydrogel flow cell chips and result interpretations, respectively. Lastly, we thank Alexander Schober from NTU Singapore for providing the Goldengate compatible pHue vector.

Funding

H.-H.K., T.W., S.M., and L.J.H. were funded by the Deutsche Forschungsgemeinschaft (DFG) SFB-TR 175, project B09, and J.N. and M.O. by SFB-TR 175, project A06. J.d.V. acknowledges funding by the DFG within the framework of MAdLand (SPP 2237), in which Z.M.A. is a PhD student (project 440231723). P.G. was supported by DFG project number 456013262. L.C.M.M. was supported by BBSRC-NSF/BIO (BB/Y000323/1) and UKRI-Future Leaders Fellowship (MR/T020679/1 and MR/Y034074/1). Confocal microscopy work was funded by DFG (INST 86/2231-1 FUGG) and (SFB-TR 175, project Z01) to H.-H.K.. Open Access funding enabled and organized by Project DEAL. K.M.S. was funded by the European Union (ERC, MITOSIZE, 101169998). Views and opinions expressed are, however, those of the author(s) only and do not necessarily reflect those of the European Union or the European Research Council. Neither the European Union nor the granting authority can be held responsible for them.

817 **Figures and Legends**

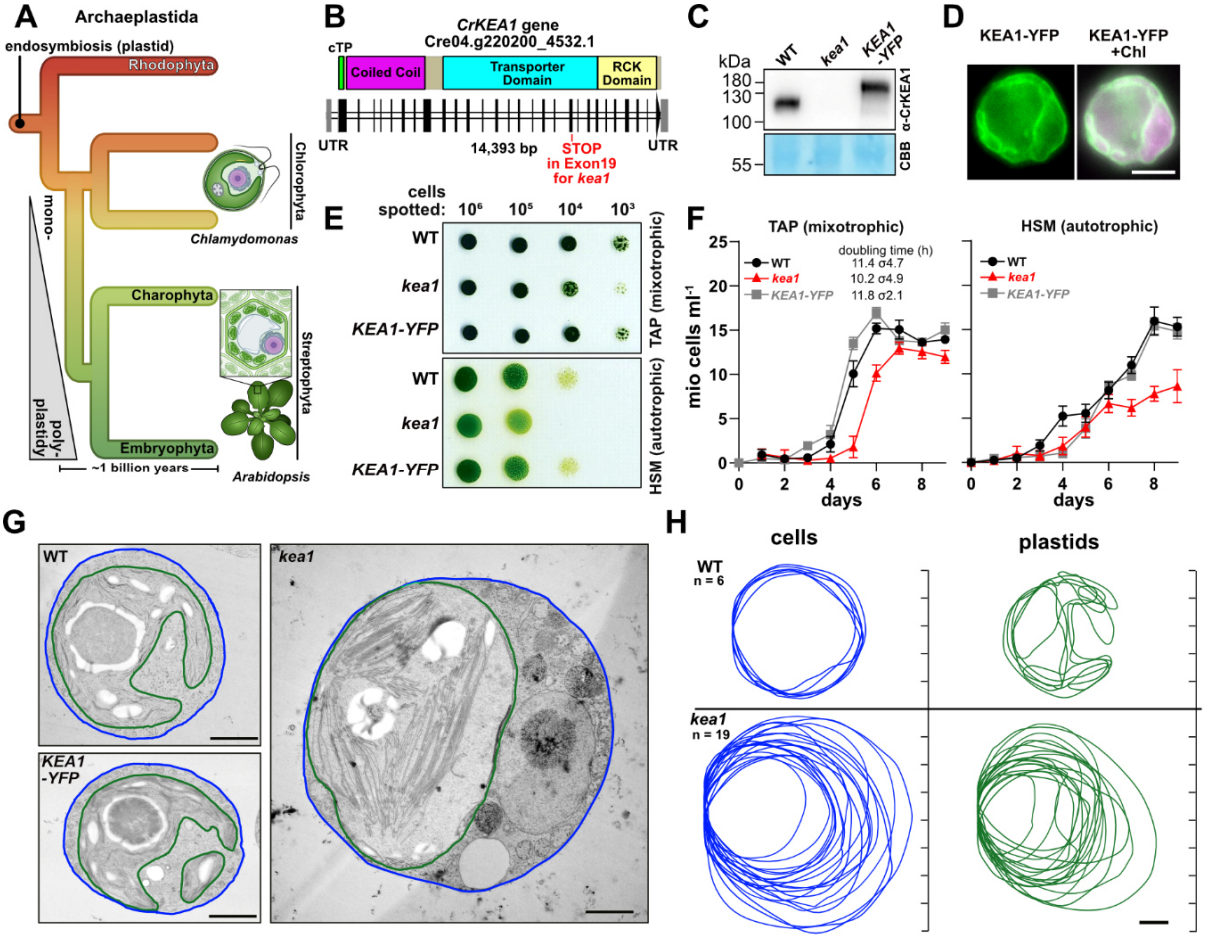

818
819 **Figure 1: Characterization of *CrKEA1* knock-out and complementation lines: growth,**
820 **localization, and cellular ultrastructure. (A)** Simplified cladogram of the Archaeplastida
821 showing the phylogenetic relationship between monoplastidic *Chlamydomonas* algae and
822 multicellular, polyplastidic *Arabidopsis* plants, both derived from a common monoplastidic
823 ancestor that diverged approximately 1 billion years ago. **(B)** Schematic of the CRISPR/Cas9
824 knock-out line *kea1*. **(C)** Immunoblot using anti-CrKEA1 antibodies on total protein extracts from
825 WT, *kea1*, and the complementation line (*CrKEA1–YFP* expressed in *kea1*). **(D)** Localization of
826 YFP-tagged CrKEA1 to the plastid envelope in the complementation line. Scale bar 5 µm. **(E)**
827 Drop cultures grown on mixotrophic (acetate-containing TAP) and photoautotrophic (HSM) solid
828 media at 25 µmol m^{-2} s^{-1}. **(F)** Growth curves (Mean±SD) of mixotrophic and photoautotrophic
829 liquid cultures at 25 µmol m^{-2} s^{-1}. σ=standard deviation. n=3. **(G)** Representative TEM images of
830 cells grown in HSM at 100 µE. Scale bar 1 µm. **(H)** Comparison of cell and chloroplast size and
831 shape based on TEM micrographs shown in panel G. Scale bar 1 µm.
832

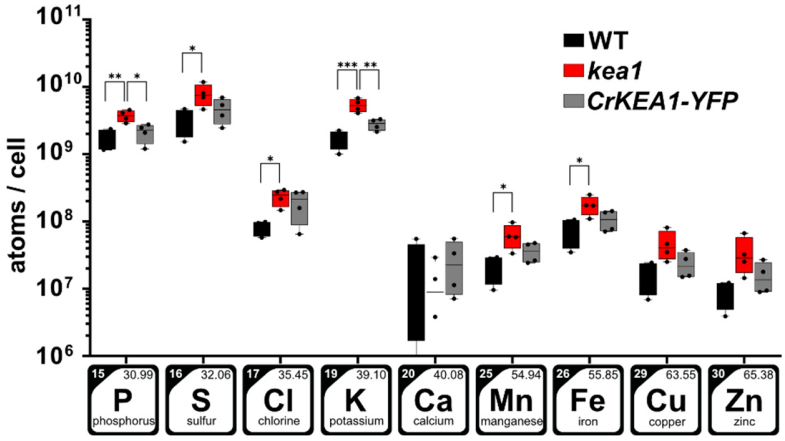

Figure 2: Ionomic profiles of Chlamydomonas *kea1* and control strains. Elemental composition of whole cells was measured by Total Reflection X-Ray Fluorescence (TXRF) from TAP liquid cultures grown at 25 µmol m^{-2} s^{-1}. Four replicate cultures per genotype were analyzed. Data were evaluated by one-way ANOVA for each element separately, and differences were assessed using Tukey's multiple comparison test. Box plots display the median (center line), the 25th to 75th percentiles (box), and the minimum and maximum values (whiskers). Asterisks indicate significant differences (* $p < 0.05$; ** $p < 0.01$; *** $p < 0.001$).

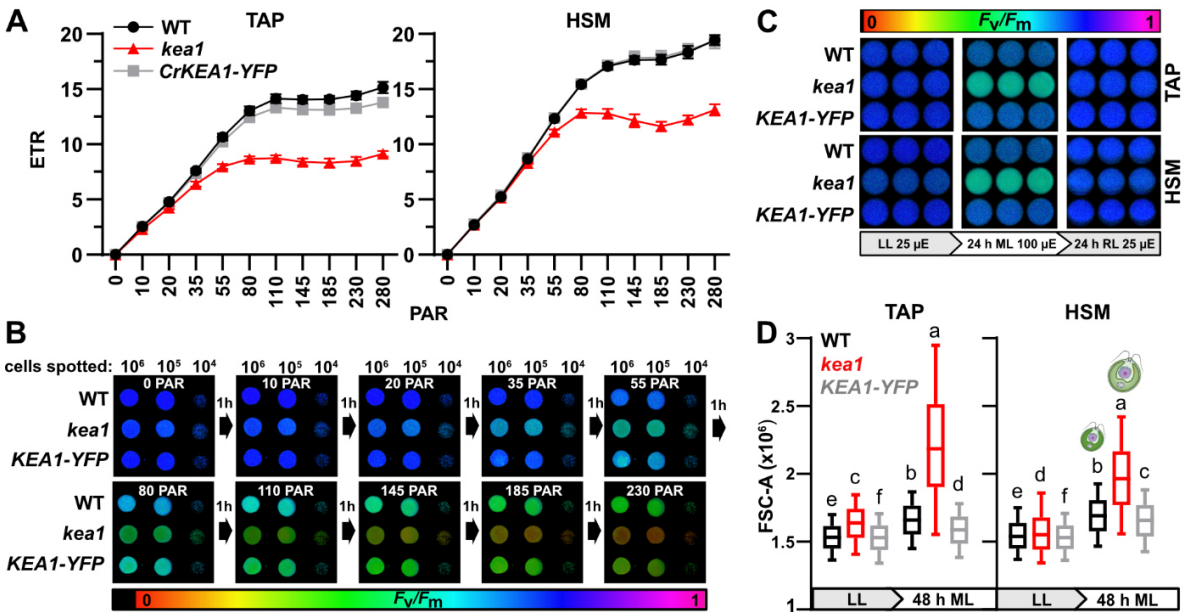

Figure 3: Photosynthetic characterization of *kea1* and cell size. (A) To assess the photosynthetic performance of *kea1*, liquid TAP and HSM cultures were exposed to gradually increasing light intensities, with PAR raised in 20-s intervals. Mean electron transfer rate (ETR) was plotted with standard deviation. n=4. **(B)** F_v/F_m values were determined from HSM drop cultures every 1 h while stepwise increasing light intensity. **(C)** Light-shift experiment with TAP and HSM liquid cultures. F_v/F_m was measured before and after transferring cultures from low light (LL) to moderate light (ML) for 24 h and back to low light for 24 h of recovery (RL). **(D)** The average cell size of *kea1* increased under moderate light (100 µmol m^{-2} s^{-1}). Chlamydomonas cultures grown in HSM or TAP at 25 µmol m^{-2} s^{-1} were shifted to 100 µmol m^{-2} s^{-1} and analyzed by flow cytometry (FC) before and 48 h after the light shift. FSC-A values correlate with cell size. Boxes represent the interquartile range, the line indicates the median, and whiskers extend to the 10th and 90th percentiles; outliers (0–10 % and 90–100 %) are not shown. Letters indicate statistical groups. Statistical analysis was performed using one-way ANOVA with Kruskal-Wallis test. All strains were pre-cultured at 25 µmol m^{-2} s^{-1} and 23 °C in TAP under shaking conditions.

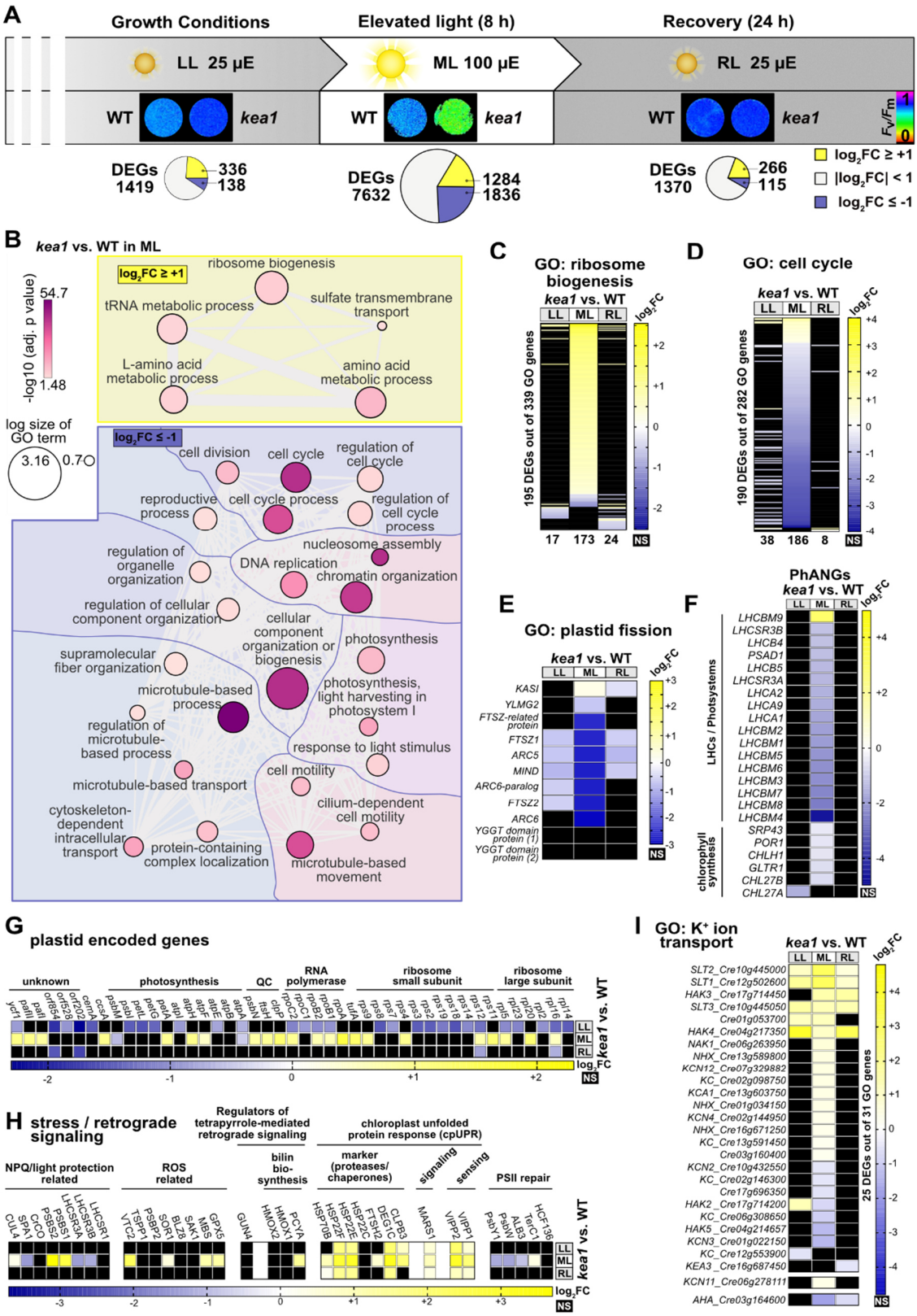
A
Growth Conditions
Elevated light (8 h)
Recovery (24 h)
LL 25 µE
ML 100 µE
RL 25 µE
WT
kea1
Fv/Fm
DEGs 1419
336
138
DEGs 7632
1284
1836
DEGs 1370
266
115
log2FC ≥ +1
|log2FC| < 1
log2FC ≤ -1
B
kea1 vs. WT in ML
-log10 (adj. p value)
54.7
1.48
log size of GO term
3.16
0.7
log2FC ≥ +1
ribosome biogenesis
tRNA metabolic process
sulfate transmembrane transport
L-amino acid metabolic process
amino acid metabolic process
log2FC ≤ -1
cell division
cell cycle
regulation of cell cycle
reproductive process
cell cycle process
regulation of cell cycle process
nucleosome assembly
regulation of organelle organization
DNA replication
chromatin organization
regulation of cellular component organization
cellular component organization or biogenesis
photosynthesis
supramolecular fiber organization
microtubule-based process
photosynthesis, light harvesting in photosystem I
regulation of microtubule-based process
response to light stimulus
cell motility
microtubule-based transport
cilium-dependent cell motility
cytoskeleton-dependent intracellular transport
protein-containing complex localization
microtubule-based movement
C
GO: ribosome biogenesis
kea1 vs. WT
LL
ML
RL
log2FC
195 DEGs out of 339 GO genes
17
173
24
NS
D
GO: cell cycle
kea1 vs. WT
190 DEGs out of 282 GO genes
38
186
8
NS
E
GO: plastid fission
kea1 vs. WT
KASI
YLMG2
FTSZ-related protein
FTSZ1
ARC5
MIND
ARC6-paralog
FTSZ2
ARC6
YGGT domain protein (1)
YGGT domain protein (2)
NS
F
PhANGs
kea1 vs. WT
LHCs / Photosystems
chlorophyll synthesis
LHCBM9
LHCSR3B
LHCB4
PSAD1
LHCB5
LHCSR3A
LHCA2
LHCA9
LHCA1
LHCBM2
LHCBM1
LHCBM5
LHCBM6
LHCBM3
LHCBM7
LHCBM8
LHCBM4
SRP43
POR1
CHLH1
GLTR1
CHL27B
CHL27A
NS
G
plastid encoded genes
unknown
photosynthesis
QC
RNA polymerase
ribosome small subunit
ribosome large subunit
kea1 vs. WT
log2FC
NS
H
stress / retrograde signaling
NPQ/light protection related
ROS related
Regulators of tetrapyrrole-mediated retrograde signaling
bilin bio-synthesis
chloroplast unfolded protein response (cpUPR)
marker (proteases/ chaperones)
signaling
sensing
PSII repair
kea1 vs. WT
log2FC
NS
I
GO: K+ ion transport
kea1 vs. WT
SLT2_Cre10g445000
SLT1_Cre12g502600
HAK3 _Cre17g714450
SLT3_Cre10g445050
Cre01g053700
HAK4_Cre04g217350
NAK1_Cre06g263950
NHX_Cre13g589800
KCN12_Cre07g329882
KC_Cre02g098750
KCA1_Cre13g603750
NHX_Cre01g034150
KCN4_Cre02g144950
NHX_Cre16g671250
KC_Cre13g591450
Cre03g160400
KCN2_Cre10g432550
KC_Cre02g146300
Cre17g696350
HAK2 _Cre17g714200
KC_Cre06g308650
HAK5 _Cre04g214657
KCN3_Cre01g022150
KC_Cre12g553900
KEA3 _Cre16g687450
KCN11_Cre06g278111
AHA_Cre03g164600
25 DEGs out of 31 GO genes
log2FC
NS

861

862 **Figure 4: RNA-seq analysis of a light-shift experiment comparing transcriptional responses**
863 **of *kea1* and WT. (A)** Experimental setup for the RNA-seq analysis, including F_v/F_m values of the
864 cultures and pie charts indicating the number of significantly differentially expressed genes
865 (DEGs; adj. p-value < 0.05) per steady-state comparison (*kea1* vs. WT). Yellow and blue sectors
866 denote up- and downregulated genes, respectively ($|\log_2 FC| \geq 1$). **(B)** Gene Ontology (GO) terms
867 of the *Biological Process* domain enriched among DEGs as interactive graph (REVIGO). **(C, D)**
868 Heatmaps showing $\log_2$FC values of significant DEGs annotated to the GO terms *ribosome*
869 *biogenesis* (GO:0042254) and *cell cycle (*GO:0007049). "GO genes" indicates the number of genes
870 associated with each respective GO term. Non-significant (NS) transcripts are not shown, or
871 displayed in black if significant under specific conditions (LL, ML, or RL). **(D, E)** Log_2FC values
872 of significant DEGs of certain GO terms (ribosome biogenesis and cell cycle) are represented as
873 heatmaps. "GO genes" refers to the number of genes annotated to the respective GO term. Not
874 significantly (NS) changed transcripts are not shown or are represented in black if they are
875 significant for a certain condition (LL, ML, or RL). **(F–H)** As in (D, E), showing $\log_2$FC values of
876 significant transcripts belonging to gene lists denoted as *plastid fission (GO:0043572),*
877 *photosynthesis-associated nuclear genes (PhANGs)*, *plastid-encoded genes*, and examples of
878 transcripts *related to stress/retrograde signaling, and ion transport (mainly including*
879 *GO:0006813 potassium ion transport). Gene names were assigned to Gene IDs using annotations*
880 *given on Phytozome. Appropriate Gene IDs are provided as supplementary data. HAK*, *NAK*, and
881 *KCN* genes were named according to Xu et al., 2016 and Li et al., 2023. Sodium hydrogen
882 exchanger, sodium/sulfate co-transporter, and potassium channels were abbreviated as *NHX*, *SLT*,
883 and *KC(N)*, respectively.
884

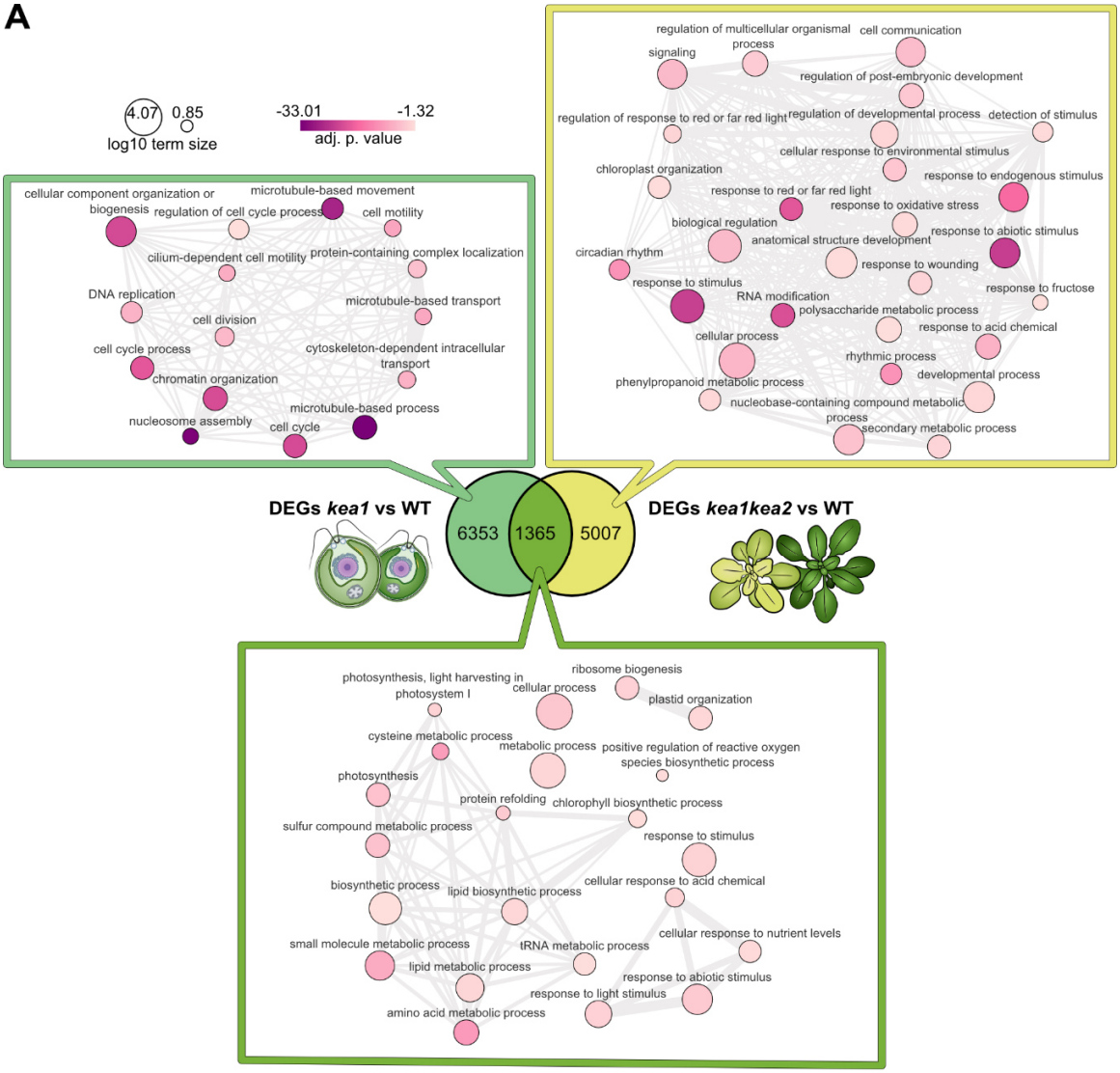
A
4.07
0.85
log10 term size
-33.01
-1.32
adj. p. value
cellular component organization or biogenesis
microtubule-based movement
regulation of cell cycle process
cell motility
cilium-dependent cell motility
protein-containing complex localization
DNA replication
microtubule-based transport
cell division
cell cycle process
cytoskeleton-dependent intracellular transport
chromatin organization
microtubule-based process
nucleosome assembly
cell cycle
regulation of multicellular organismal process
cell communication
signaling
regulation of post-embryonic development
regulation of response to red or far red light
regulation of developmental process
detection of stimulus
cellular response to environmental stimulus
chloroplast organization
response to endogenous stimulus
response to red or far red light
response to oxidative stress
biological regulation
response to abiotic stimulus
anatomical structure development
circadian rhythm
response to wounding
response to stimulus
response to fructose
RNA modification
polysaccharide metabolic process
cellular process
response to acid chemical
rhythmic process
developmental process
phenylpropanoid metabolic process
nucleobase-containing compound metabolic process
secondary metabolic process
DEGs kea1 vs WT
6353
1365
5007
DEGs kea1kea2 vs WT
photosynthesis, light harvesting in photosystem I
ribosome biogenesis
cellular process
plastid organization
cysteine metabolic process
metabolic process
positive regulation of reactive oxygen species biosynthetic process
photosynthesis
protein refolding
chlorophyll biosynthetic process
sulfur compound metabolic process
response to stimulus
biosynthetic process
lipid biosynthetic process
cellular response to acid chemical
cellular response to nutrient levels
small molecule metabolic process
tRNA metabolic process
lipid metabolic process
response to abiotic stimulus
response to light stimulus
amino acid metabolic process

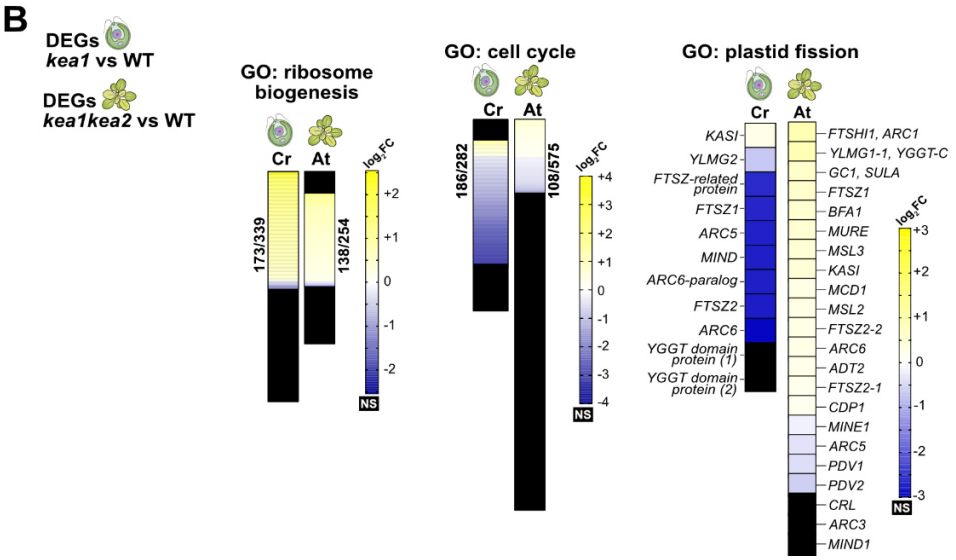
B
DEGs kea1 vs WT
DEGs kea1kea2 vs WT
GO: ribosome biogenesis
Cr
At
173/339
138/254
log2FC
+2
+1
0
-1
-2
NS
GO: cell cycle
Cr
At
186/282
108/575
log2FC
+4
+3
+2
+1
0
-1
-2
-3
-4
NS
GO: plastid fission
Cr
At
KASI
YLMG2
FTSZ-related protein
FTSZ1
ARC5
MIND
ARC6-paralog
FTSZ2
ARC6
YGGT domain protein (1)
YGGT domain protein (2)
FTSHI1, ARC1
YLMG1-1, YGGT-C
GC1, SULA
FTSZ1
BFA1
MURE
MSL3
KASI
MCD1
MSL2
FTSZ2-2
ARC6
ADT2
FTSZ2-1
CDP1
MINE1
ARC5
PDV1
PDV2
CRL
ARC3
MIND1
log2FC
+3
+2
+1
0
-1
-2
-3
NS

885

886 **Figure 5: Cross-species transcriptomic comparison of inner envelope *KEA* mutants in**
887 **Chlamydomonas and Arabidopsis**. **(A)** Mutants lacking inner envelope *KEA* transporters
888 (Chlamydomonas *kea1* and Arabidopsis *kea1kea2*) in both Chlamydomonas and Arabidopsis share
889 a subset of differentially expressed genes (DEGs). Shared DEGs were identified by mapping
890 Chlamydomonas genes to Arabidopsis orthologs using g:Orth. Significant DEGs (adj.
891 p-value < 0.05; numbers shown in the Venn diagram) were filtered using $|\log_2 FC| \geq 0.75$ and
892 subjected to Gene Ontology (GO) enrichment analysis with g:Profiler (*Biological Process*
893 domain). GO terms are shown as interactive graph (REVIGO). Chlamydomonas DEGs correspond
894 to the moderate light (ML) condition. Shared DEGs are enriched for *ribosome biogenesis*
895 (GO:0042254), whereas enrichment for *cell cycle* (GO:0007049) is observed only in
896 Chlamydomonas. **(B)** Heatmaps display $\log_2 FC$ values for all genes annotated to *ribosome*
897 *biogenesis*. Only significant DEGs (adj. p-value < 0.05) are color-coded, while non-significant
898 (NS) or undetected genes are shown in black. Numbers indicate the count of significant DEGs
899 relative to the total number of genes annotated to the respective GO term (DEGs / GO term size).

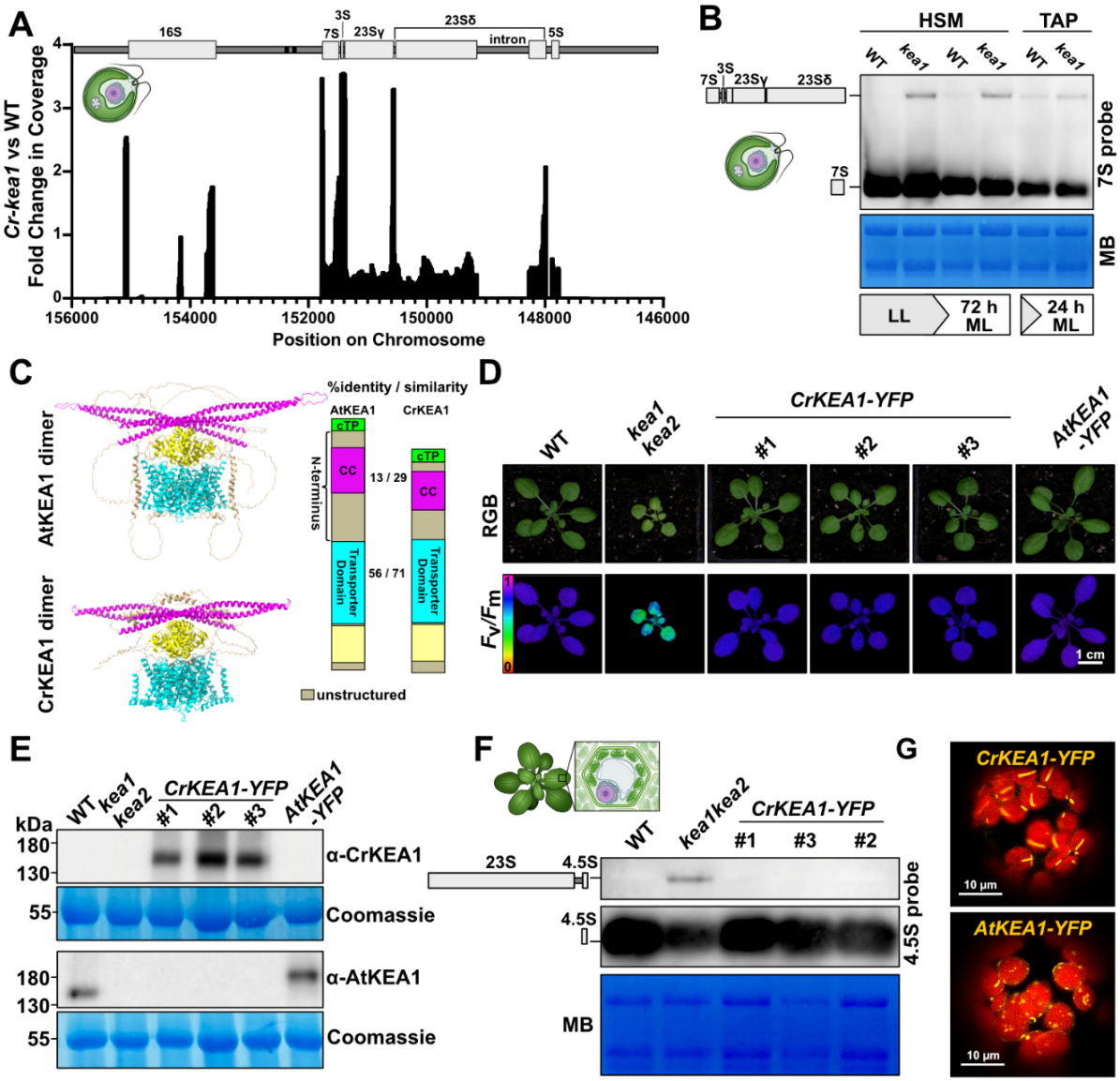

Figure 6: Conserved role of inner envelope KEA transporters in plastid rRNA processing across algae and higher plants. (A) Impaired plastid rRNA processing in *kea1* leads to enrichment of the 7S–3S–23S precursor. Shown is the fold change in normalized read coverage (*BamCompare*) from an rRNA-seq experiment comparing *kea1* and WT, revealing increased read density over intergenic regions corresponding to the 7S–3S–23S precursor in the mutant. **(B)** RNA blot analysis using specific plastid rRNA probes confirms accumulation of the 7S–3S–23S precursor in *kea1*. MB, Methylene Blue. **(C)** Structural comparison of AtKEA1 and CrKEA1. AlphaFold3 models of dimeric AtKEA1 and its algal homolog CrKEA1 are shown, with colors corresponding to domain organization depicted to the right. The representation as a dimer was chosen due to the structural findings for the bacterial homolog KefC (Gulati et al., 2024). **(D)** Phenotypical complementation of the Arabidopsis *kea1kea2* mutant by expressing *CrKEA1–YFP*. Scale bar 1cm. **(E)** Immunoblot validation of *CrKEA1–YFP* expression in complementation lines. **(F)** RNA blot demonstrating restoration of normal plastid rRNA processing in *kea1kea2* upon

expression of *CrKEA1–YFP*. MB, Methylene Blue. **(G)** Confocal microscopy of protoplasts isolated from *kea1kea2* plants expressing either *AtKEA1–YFP* or *CrKEA1–YFP*. Chlorophyll autofluorescence (*red*) and YFP signal (*yellow*) displayed in false colors. Scale bar 10 µm.

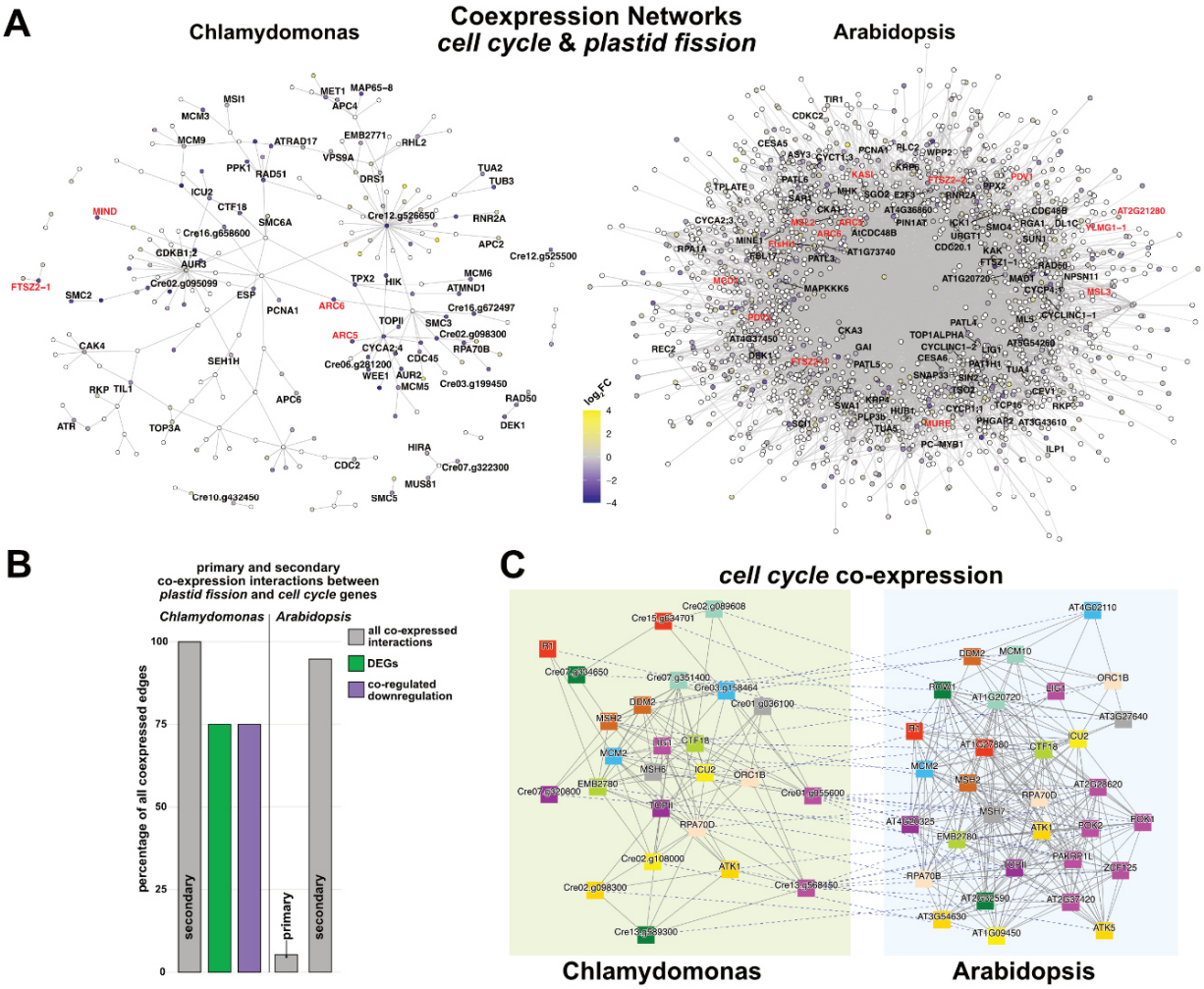

Figure 7: Comparisons between co-expression networks of Arabidopsis and Chlamydomonas. (A) From both species, genes annotated to GO:0007049 (*cell cycle*) and GO:0043572 (*plastid fission*) were extracted and visualized based on co-expression relationships in each species. Nodes represent genes and edges connect co-expressed genes. Gene names are black for *cell cycle* and red for *plastid fission*. Nodes represent genes, and edges connect co-expressed genes. White nodes indicate genes that were not significantly changed or not detected; gradient-colored nodes represent DEGs, with color intensity reflecting $\log_2$FC. ML DEGs were used for Chlamydomonas. **(B)** Primary and secondary co-expression interactions between *plastid fission* and *cell cycle* genes found in the networks. Co-regulated downregulation is based on both genes being downregulated DEGs. Cut-off $|\log_2 FC| \geq 0.75$. **(C)** Comparative co-expression network analysis of a *cell cycle* clusters. Nodes represent genes, solid edges connect co-expressed genes and dashed edges connect orthologues. Coloured shapes represent different orthogroups. Cluster comparisons were based on Jaccard Index (JI) computation.

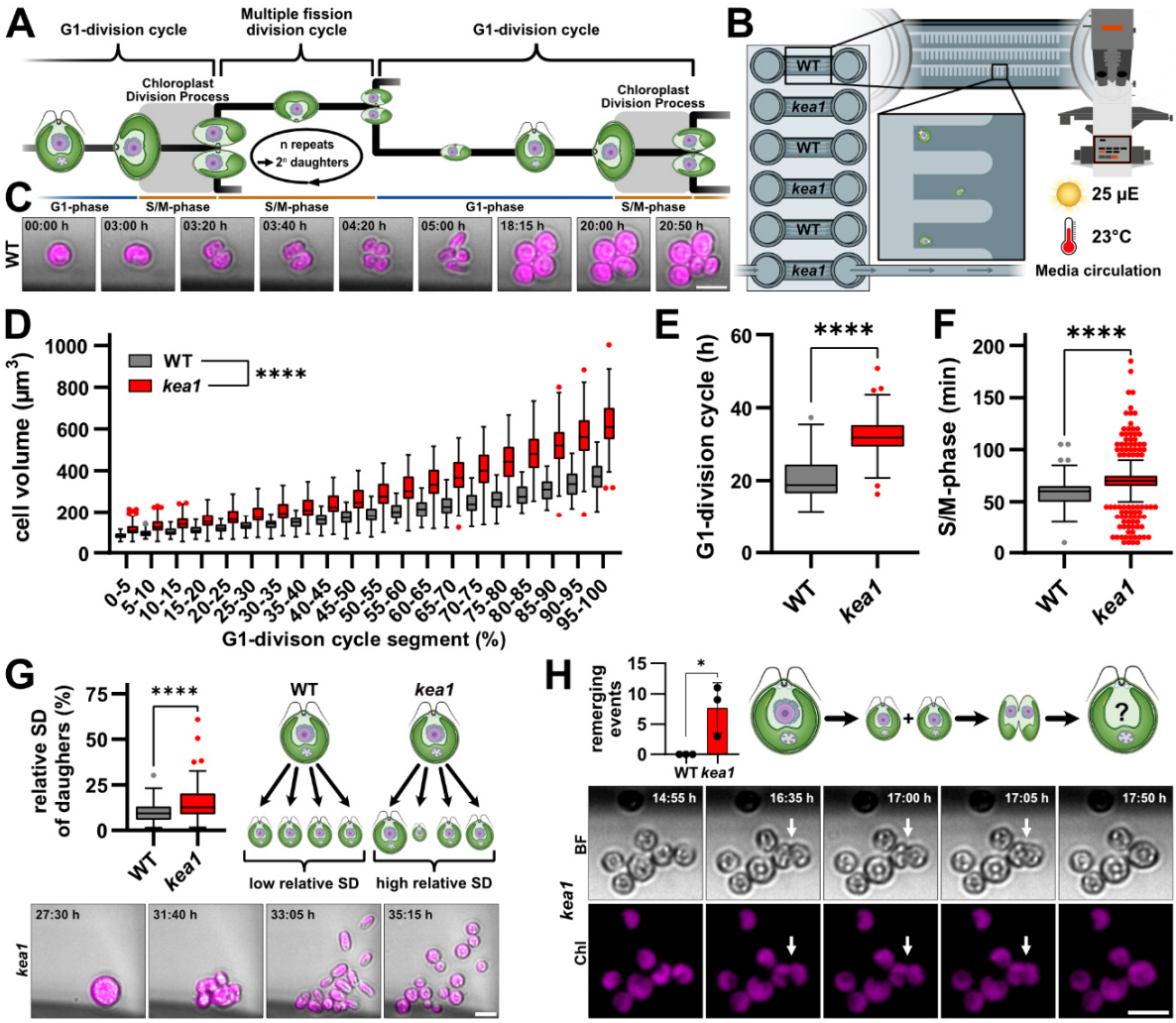

933

934 **Figure 8: Single Cell Live Imaging reveals cell cycle defects of *kea1*. (A)** Simplified diagram of the
935 Chlamydomonas cell cycle, **showing the labeling of cell-cycle phases used in this study. (B)** Schematic
936 of the microfluidic flow-cell chip containing hydrogel-based channels with imprinted cavities that
937 immobilize multiple individual cells for long-term observation. **(C)** Representative time-lapse image series
938 of WT cells illustrating synchronized growth and division. **(D–F)** Quantitative analysis of single-cell
939 trajectories shows that *kea1* cells exhibit significantly increased cell volume in every G1-division cycle
940 segment, prolonged G1 phase, and extended S/M phase compared to WT. **(G)** *kea1* daughter cells display
941 greater size variation following division than WT. **(H)** "Remerging" events—where nearly separated
942 daughter cells fuse again—occur more frequently in *kea1* and were not observed in WT. The bar graph
943 summarizes data from three replicate channels per genotype. *For all panels:* Representative time-lapse
944 series are shown. Scale bars, 10 µm. Box plots follow Tukey's convention. Statistical significance was
945 determined with Mann-Whitney tests (D-G) and unpaired t-test (H) and is indicated by asterisks (* $p < 0.05$;
946 ** $p < 0.01$; *** $p < 0.001$; **** $p < 0.0001$).

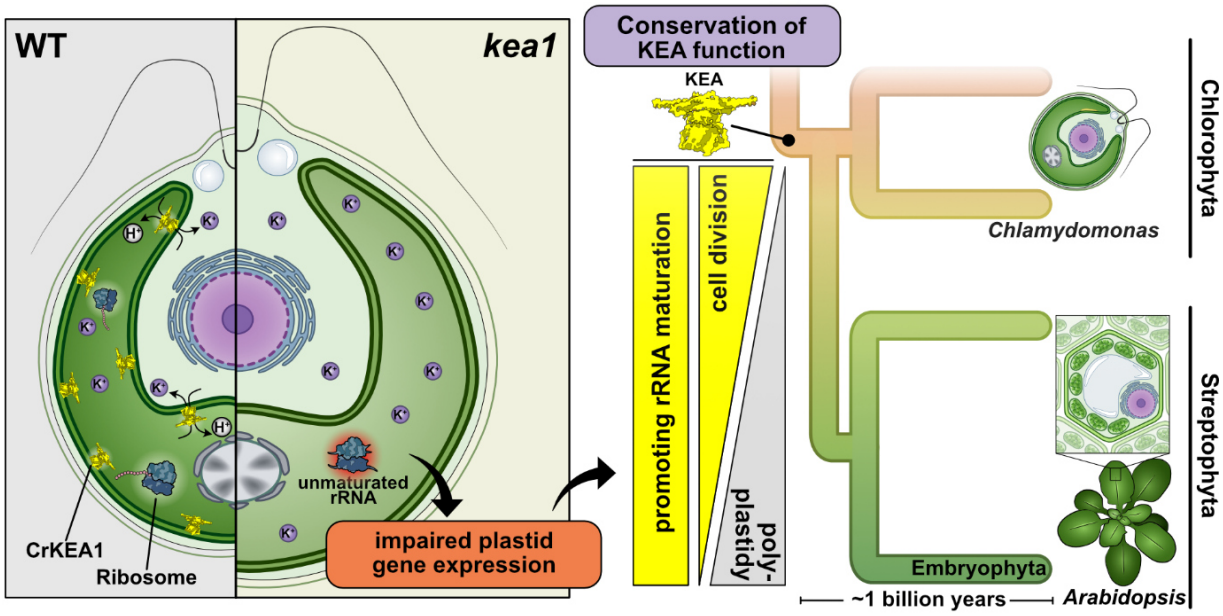

Figure 9: Model: Conserved role of inner envelope KEA transporters across the green lineage.

In Chlamydomonas, loss of the inner envelope KEA transporters (IE KEAs) leads to potassium imbalance and excess stromal K^+, resulting in swollen, misshapen chloroplasts and impaired rRNA processing required for plastid ribosome biogenesis. IE KEAs, including CrKEA1 in Chlamydomonas and AtKEA1/2 in Arabidopsis, are conserved throughout the green branch of the Archaeplastida, spanning the Chlorophyta (green algae) and Streptophyta (charophytes and land plants). All lineages evolved from a monoplastidic unicellular ancestor characterized by tightly coupled plastid and cell division (*monoplastidic bottleneck*, de Vries and Gould, 2018), a condition still retained in Chlamydomonas. During evolution, the emergence of multicellularity and polyplastidy, as in Arabidopsis, relaxed this coupling and allowed plastid division to proceed independently of the cell cycle. Our findings suggest that the importance of IE KEA-mediated ion homeostasis for error-free cell division diminished with the transition to polyplastidy, while its role in maintaining proper rRNA maturation and ribosome assembly remains conserved across Chlorophyta and Streptophyta.

References

Abramson J, Adler J, Dunger J, Evans R, Green T, Pritzel A, Ronneberger O, Willmore L, Ballard AJ, Bambrick J, Bodenstein SW, Evans DA, Hung CC, O'Neill M, Reiman D, Tunyasuvunakool K, Wu Z, Žemgulytė A, Arvaniti E, Beattie C, Bertolli O, Bridgland A, Cherepanov A, Congreve M, Cowen-Rivers AI, Cowie A, Figurnov M, Fuchs FB, Gladman H, Jain R, Khan YA, Low CMR, Perlin K, Potapenko A, Savy P, Singh S, Stecula A, Thillaisundaram A, Tong C, Yakneen S, Zhong ED, Zielinski M, Žídek A, Bapst V, Kohli P, Jaderberg M, Hassabis D, Jumper JM (2024) Accurate structure prediction of biomolecular interactions with AlphaFold 3. Nature **630:** 493-500

Ahmed T, Yin Z, Bhushan S (2016) Cryo-EM structure of the large subunit of the spinach chloroplast ribosome. Sci Rep **6:** 35793

Aihara Y, Fujimura-Kamada K, Yamasaki T, Minagawa J (2019) Algal photoprotection is regulated by the E3 ligase CUL4-DDB1(DET1). Nat Plants **5:** 34-40

Aranda-Sicilia MN, Aboukila A, Armbruster U, Cagnac O, Schumann T, Kunz HH, Jahns P, Rodríguez-Rosales MP, Sze H, Venema K (2016) Envelope K+/H+ Antiporters AtKEA1 and AtKEA2 Function in Plastid Development. Plant Physiol **172:** 441-449

Baker RT, Catanzariti AM, Karunasekara Y, Soboleva TA, Sharwood R, Whitney S, Board PG (2005) Using deubiquitylating enzymes as research tools. Methods Enzymol **398:** 540-554

Bialevich V, Zachleder V, Bišová K (2022) The Effect of Variable Light Source and Light Intensity on the Growth of Three Algal Species. Cells **11**

Bierenbroodspot MJ, Darienko T, de Vries S, Delwiche CF, Lorenz M, Ali Z, Irisarri I, Pröschold T, de Vries J (2025) Phylogenomics unveil a recent origin of morphological complexity in Coleochaetophyceae. Curr Biol **35:** 5071-5080.e5077

Bisova K, Krylov DM, Umen JG (2005) Genome-wide annotation and expression profiling of cell cycle regulatory genes in Chlamydomonas reinhardtii. Plant Physiol **137:** 475-491

Bölter B, Mitterreiter MJ, Schwenkert S, Finkemeier I, Kunz HH (2020) The topology of plastid inner envelope potassium cation efflux antiporter KEA1 provides new insights into its regulatory features. Photosynth Res **145:** 43-54

Castandet B, Hotto AM, Strickler SR, Stern DB (2016) ChloroSeq, an Optimized Chloroplast RNA-Seq Bioinformatic Pipeline, Reveals Remodeling of the Organellar Transcriptome Under Heat Stress. G3 (Bethesda) **6:** 2817-2827

Catanzariti AM, Soboleva TA, Jans DA, Board PG, Baker RT (2004) An efficient system for high-level expression and easy purification of authentic recombinant proteins. Protein Sci **13:** 1331-1339

Catherall E, Musial S, Atkinson N, Walker CE, Mackinder LCM, McCormick AJ (2025) From algae to plants: understanding pyrenoid-based CO(2)-concentrating mechanisms. Trends Biochem Sci **50:** 33-45

Chanroj S, Wang G, Venema K, Zhang MW, Delwiche CF, Sze H (2012) Conserved and diversified gene families of monovalent cation/h(+) antiporters from algae to flowering plants. Front Plant Sci **3:** 25

Clark-Cotton MR, Chen SA, Gomez A, Mulabagal AJ, Perry A, Malhotra V, Onishi M (2025) Imaging-based screen identifies novel natural compounds that perturb cell and chloroplast division in Chlamydomonas reinhardtii. Mol Biol Cell **36:** br14

1009 **Clough SJ, Bent AF** (1998) Floral dip: a simplified method for Agrobacterium-mediated
1010 transformation of Arabidopsis thaliana. Plant J **16:** 735-743
1011 **Cross FR, Umen JG** (2015) The Chlamydomonas cell cycle. Plant J **82:** 370-392
1012 **Dadras A, Fürst-Jansen JMR, Darienko T, Krone D, Scholz P, Sun S, Herrfurth C, Rieseberg**
1013 **TP, Irisarri I, Steinkamp R, Hansen M, Buschmann H, Valerius O, Braus GH,**
1014 **Hoecker U, Feussner I, Mutwil M, Ischebeck T, de Vries S, Lorenz M, de Vries J**
1015 (2023) Environmental gradients reveal stress hubs pre-dating plant terrestrialization. Nat
1016 Plants **9:** 1419-1438
1017 **Davies DR, Lyall V** (1973) The assembly of a highly ordered component of the cell wall: The role
1018 of heritable factors and of physical structure. Molecular and General Genetics MGG **124:**
1019 21-34
1020 **de Vries J, Gould SB** (2018) The monoplastidic bottleneck in algae and plant evolution. J Cell
1021 Sci **131**
1022 **DeTar RA, Barahimipour R, Manavski N, Schwenkert S, Höhner R, Bölter B, Inaba T,**
1023 **Meurer J, Zoschke R, Kunz HH** (2021) Loss of inner-envelope K+/H+ exchangers
1024 impairs plastid rRNA maturation and gene expression. Plant Cell **33:** 2479-2505
1025 **DeTar RA, Höhner R, Manavski N, Blackholm M, Meurer J, Kunz HH** (2022) Loss of SALT
1026 OVERLY SENSITIVE 1 prevents virescence in chloroplast K+/H+ EFFLUX
1027 ANTIPORTER-deficient mutants. Plant Physiol **189:** 1220-1225
1028 **Dogra V, Duan J, Lee KP, Kim C** (2019) Impaired PSII proteostasis triggers a UPR-like response
1029 in the var2 mutant of Arabidopsis. J Exp Bot **70:** 3075-3088
1030 **Duanmu D, Casero D, Dent RM, Gallaher S, Yang W, Rockwell NC, Martin SS, Pellegrini**
1031 **M, Niyogi KK, Merchant SS, Grossman AR, Lagarias JC** (2013) Retrograde bilin
1032 signaling enables Chlamydomonas greening and phototrophic survival. Proc Natl Acad Sci
1033 U S A **110:** 3621-3626
1034 **Dupuis S, Ojeda V, Gallaher SD, Purvine SO, Glaesener AG, Ponce R, Nicora CD,**
1035 **Bloodsworth K, Lipton MS, Niyogi KK, Iwai M, Merchant SS** (2025) Too dim, too
1036 bright, and just right: Systems analysis of the Chlamydomonas diurnal program under
1037 limiting and excess light. Plant Cell **37**
1038 **Dutcher SK, Li L, Lin H, Meyer L, Giddings TH, Jr., Kwan AL, Lewis BL** (2012) Whole-
1039 Genome Sequencing to Identify Mutants and Polymorphisms in Chlamydomonas
1040 reinhardtii. G3 (Bethesda) **2:** 15-22
1041 **Emrich-Mills TZ, Yates G, Barrett J, Girr P, Grouneva I, Lau CS, Walker CE, Kwok TK,**
1042 **Davey JW, Johnson MP, Mackinder LCM** (2021) A recombineering pipeline to clone
1043 large and complex genes in Chlamydomonas. Plant Cell **33:** 1161-1181
1044 **Fauser F, Vilarrasa-Blasi J, Onishi M, Ramundo S, Patena W, Millican M, Osaki J, Philp C,**
1045 **Nemeth M, Salomé PA, Li X, Wakao S, Kim RG, Kaye Y, Grossman AR, Niyogi KK,**
1046 **Merchant SS, Cutler SR, Walter P, Dinneny JR, Jonikas MC, Jinkerson RE** (2022)
1047 Systematic characterization of gene function in the photosynthetic alga Chlamydomonas
1048 reinhardtii. Nat Genet **54:** 705-714
1049 **Feeney KA, Hansen LL, Putker M, Olivares-Yañez C, Day J, Eades LJ, Larrondo LF, Hoyle**
1050 **NP, O'Neill JS, van Ooijen G** (2016) Daily magnesium fluxes regulate cellular
1051 timekeeping and energy balance. Nature **532:** 375-379
1052 **Gabilly ST, Baker CR, Wakao S, Crisanto T, Guan K, Bi K, Guiet E, Guadagno CR, Niyogi**
1053 **KK** (2019) Regulation of photoprotection gene expression in Chlamydomonas by a

putative E3 ubiquitin ligase complex and a homolog of CONSTANS. Proc Natl Acad Sci U S A **116:** 17556-17562

Galaxy-Community (2024) The Galaxy platform for accessible, reproducible, and collaborative data analyses: 2024 update. Nucleic Acids Res **52:** W83-w94

Gallusser B, Weigert M (2025) TRACKASTRA: Transformer-Based Cell Tracking for Live-Cell Microscopy. *In*. Springer Nature Switzerland, Cham, pp 467-484

Gorman DS, Levine RP (1965) Cytochrome f and plastocyanin: their sequence in the photosynthetic electron transport chain of Chlamydomonas reinhardi. Proc Natl Acad Sci U S A **54:** 1665-1669

Greiner A, Kelterborn S, Evers H, Kreimer G, Sizova I, Hegemann P (2017) Targeting of Photoreceptor Genes in Chlamydomonas reinhardtii via Zinc-Finger Nucleases and CRISPR/Cas9. Plant Cell **29:** 2498-2518

Grossman AR, Karpowicz SJ, Heinnickel M, Dewez D, Hamel B, Dent R, Niyogi KK, Johnson X, Alric J, Wollman FA, Li H, Merchant SS (2010) Phylogenomic analysis of the Chlamydomonas genome unmasks proteins potentially involved in photosynthetic function and regulation. Photosynth Res **106:** 3-17

Gulati A, Kokane S, Perez-Boerema A, Alleva C, Meier PF, Matsuoka R, Drew D (2024) Structure and mechanism of the K(+)/H(+) exchanger KefC. Nat Commun **15:** 4751

Gutman BL, Niyogi KK (2004) Chlamydomonas and Arabidopsis. A dynamic duo. Plant Physiol **135:** 607-610

Harris EH, Stern DB, Witman G (2009) The chlamydomonas sourcebook, Vol 1. Elsevier San Diego, CA

Henslee EA, Crosby P, Kitcatt SJ, Parry JSW, Bernardini A, Abdallat RG, Braun G, Fatoyinbo HO, Harrison EJ, Edgar RS, Hoettges KF, Reddy AB, Jabr RI, von Schantz M, O'Neill JS, Labeed FH (2017) Rhythmic potassium transport regulates the circadian clock in human red blood cells. Nat Commun **8:** 1978

Höhner R, Galvis VC, Strand DD, Völkner C, Krämer M, Messer M, Dinc F, Sjuts I, Bölter B, Kramer DM, Armbruster U, Kunz H-H (2019) Photosynthesis in Arabidopsis Is Unaffected by the Function of the Vacuolar K+ Channel TPK3. Plant Physiology **180:** 1322-1335

Holloway SP, Herrin DL (1998) Processing of a Composite Large Subunit rRNA: Studies with Chlamydomonas Mutants Deficient in Maturation of the 23S-like rRNA. The Plant Cell **10:** 1193-1206

Holtsmark I, Lee S, Lunde KA, Auestad K, Maple-Grødem J, Møller SG (2013) Plastid division control: the PDV proteins regulate DRP5B dynamin activity. Plant Mol Biol **82:** 255-266

Holzner LJ, Frank LÖ, Mühlbauer S, Müller A, Schröder L, DeTar RA, Philippar K, Mendoza-Cózatl D, Krämer U, Nägele T, Bölter B, Kunz H-H (2025) The chloroplast ionome shines new light on organellar Fe homeostasis. bioRxiv**:** 2025.2007.2028.667122

Honkanen S, Small I (2022) The GENOMES UNCOUPLED1 protein has an ancient, highly conserved role but not in retrograde signalling. New Phytol **236:** 99-113

Hotto AM, Castandet B, Gilet L, Higdon A, Condon C, Stern DB (2015) Arabidopsis chloroplast mini-ribonuclease III participates in rRNA maturation and intron recycling. Plant Cell **27:** 724-740

Kelterborn S, Boehning F, Sizova I, Baidukova O, Evers H, Hegemann P (2022) Gene Editing in Green Alga Chlamydomonas reinhardtii via CRISPR-Cas9 Ribonucleoproteins. Methods Mol Biol **2379:** 45-65

Kindle KL (1990) High-frequency nuclear transformation of Chlamydomonas reinhardtii. Proc Natl Acad Sci U S A **87:** 1228-1232

Klein DJ, Moore PB, Steitz TA (2004) The contribution of metal ions to the structural stability of the large ribosomal subunit. Rna **10:** 1366-1379

Knoblauch J, Waadt R, Cousins AB, Kunz HH (2024) Probing the in situ volumes of Arabidopsis leaf plastids using three-dimensional confocal and scanning electron microscopy. Plant J **117:** 332-341

Kolberg L, Raudvere U, Kuzmin I, Adler P, Vilo J, Peterson H (2023) g:Profiler-interoperable web service for functional enrichment analysis and gene identifier mapping (2023 update). Nucleic Acids Res **51:** W207-w212

Kunz HH, Armbruster U, Mühlbauer S, de Vries J, Davis GA (2024) Chloroplast ion homeostasis - what do we know and where should we go? New Phytol **243:** 543-559

Kunz HH, Gierth M, Herdean A, Satoh-Cruz M, Kramer DM, Spetea C, Schroeder JI (2014) Plastidial transporters KEA1, -2, and -3 are essential for chloroplast osmoregulation, integrity, and pH regulation in Arabidopsis. Proc Natl Acad Sci U S A **111:** 7480-7485

Lauersen KJ, Willamme R, Coosemans N, Joris M, Kruse O, Remacle C (2016) Peroxisomal microbodies are at the crossroads of acetate assimilation in the green microalga Chlamydomonas reinhardtii. Algal Research **16:** 266-274

Li W, Zhang Y, Ren H, Wang Z, OuYang Y, Wang S, Hussain J, Zeb I, Kong Y, Liu S, Qi G (2023) Identification of potassium transport proteins in algae and determination of their role under salt and saline-alkaline stress. Algal Research **69:** 102923

Li X, Zhang R, Patena W, Gang SS, Blum SR, Ivanova N, Yue R, Robertson JM, Lefebvre PA, Fitz-Gibbon ST, Grossman AR, Jonikas MC (2016) An Indexed, Mapped Mutant Library Enables Reverse Genetics Studies of Biological Processes in Chlamydomonas reinhardtii. Plant Cell **28:** 367-387

Li Y, Liu D, López-Paz C, Olson BJSC, Umen JG (2016) A new class of cyclin dependent kinase in Chlamydomonas is required for coupling cell size to cell division. eLife **5:** e10767

Lübben MK, Klingl A, Nickelsen J, Ostermeier M (2024) CLEM, a universal tool for analyzing structural organization in thylakoid membranes. Physiol Plant **176:** e14417

Merchant SS, Schmollinger S, Strenkert D, Moseley JL, Blaby-Haas CE (2020) From economy to luxury: Copper homeostasis in Chlamydomonas and other algae. Biochim Biophys Acta Mol Cell Res **1867:** 118822

Miyagishima SY, Froehlich JE, Osteryoung KW (2006) PDV1 and PDV2 mediate recruitment of the dynamin-related protein ARC5 to the plastid division site. Plant Cell **18:** 2517-2530

Murashige T, Skoog F (1962) A Revised Medium for Rapid Growth and Bio Assays with Tobacco Tissue Cultures. Physiologia Plantarum **15:** 473-497

Neupert J, Karcher D, Bock R (2009) Generation of Chlamydomonas strains that efficiently express nuclear transgenes. Plant J **57:** 1140-1150

Nierhaus KH (2014) Mg2+, K+, and the ribosome. Journal of bacteriology **196:** 3817-3819

Niyogi KK (1999) PHOTOPROTECTION REVISITED: Genetic and Molecular Approaches. Annu Rev Plant Physiol Plant Mol Biol **50:** 333-359

Okazaki K, Kabeya Y, Suzuki K, Mori T, Ichikawa T, Matsui M, Nakanishi H, Miyagishima SY (2009) The PLASTID DIVISION1 and 2 components of the chloroplast division

1144 machinery determine the rate of chloroplast division in land plant cell differentiation. Plant
1145 Cell **21:** 1769-1780
1146 **Pachitariu M, Stringer C** (2022) Cellpose 2.0: how to train your own model. Nat Methods **19:**
1147 1634-1641
1148 **Padovani F, Mairhörmann B, Falter-Braun P, Lengefeld J, Schmoller KM** (2022)
1149 Segmentation, tracking and cell cycle analysis of live-cell imaging data with Cell-ACDC.
1150 BMC Biol **20:** 174
1151 **Perlaza K, Toutkoushian H, Boone M, Lam M, Iwai M, Jonikas MC, Walter P, Ramundo S**
1152 (2019) The Mars1 kinase confers photoprotection through signaling in the chloroplast
1153 unfolded protein response. Elife **8**
1154 **Peschke M, Moog D, Klingl A, Maier UG, Hempel F** (2013) Evidence for glycoprotein transport
1155 into complex plastids. Proc Natl Acad Sci U S A **110:** 10860-10865
1156 **Pettersen EF, Goddard TD, Huang CC, Meng EC, Couch GS, Croll TI, Morris JH, Ferrin**
1157 **TE** (2021) UCSF ChimeraX: Structure visualization for researchers, educators, and
1158 developers. Protein Sci **30:** 70-82
1159 **Pootakham W, Gonzalez-Ballester D, Grossman AR** (2010) Identification and regulation of
1160 plasma membrane sulfate transporters in Chlamydomonas. Plant Physiol **153:** 1653-1668
1161 **Ramírez F, Ryan DP, Grüning B, Bhardwaj V, Kilpert F, Richter AS, Heyne S, Dündar F,**
1162 **Manke T** (2016) deepTools2: a next generation web server for deep-sequencing data
1163 analysis. Nucleic Acids Res **44:** W160-165
1164 **Ramkissoon SH, Mainwaring LA, Sloand EM, Young NS, Kajigaya S** (2006) Nonisotopic
1165 detection of microRNA using digoxigenin labeled RNA probes. Mol Cell Probes **20:** 1-4
1166 **Ramundo S, Casero D, Mühlhaus T, Hemme D, Sommer F, Crèvecoeur M, Rahire M,**
1167 **Schroda M, Rusch J, Goodenough U, Pellegrini M, Perez-Perez ME, Crespo JL,**
1168 **Schaad O, Civic N, Rochaix JD** (2014) Conditional Depletion of the Chlamydomonas
1169 Chloroplast ClpP Protease Activates Nuclear Genes Involved in Autophagy and Plastid
1170 Protein Quality Control. Plant Cell **26:** 2201-2222
1171 **Ramundo S, Rahire M, Schaad O, Rochaix JD** (2013) Repression of essential chloroplast genes
1172 reveals new signaling pathways and regulatory feedback loops in chlamydomonas. Plant
1173 Cell **25:** 167-186
1174 **Renna L, Papini A, Mancuso S, Brandizzi F, Stefano G** (2025) Plant Plastids: From
1175 Evolutionary Origins to Functional Specialization and Organelle Interactions. J Exp Bot
1176 **Reynolds ES** (1963) The use of lead citrate at high pH as an electron-opaque stain in electron
1177 microscopy. J Cell Biol **17:** 208-212
1178 **Richter AS, Nägele T, Grimm B, Kaufmann K, Schroda M, Leister D, Kleine T** (2023)
1179 Retrograde signaling in plants: A critical review focusing on the GUN pathway and
1180 beyond. Plant Commun **4:** 100511
1181 **Rodríguez SG, Crosby P, Hansen LL, Grünewald E, Beale AD, Spangler RK, Rabbitts BM,**
1182 **Partch CL, Stangherlin A, O'Neill JS, van Ooijen G** (2024) Potassium rhythms couple
1183 the circadian clock to the cell cycle. bioRxiv
1184 **Rozov A, Khusainov I, El Omari K, Duman R, Mykhaylyk V, Yusupov M, Westhof E,**
1185 **Wagner A, Yusupova G** (2019) Importance of potassium ions for ribosome structure and
1186 function revealed by long-wavelength X-ray diffraction. Nature communications **10:** 2519
1187 **Sager R, Zalokar M** (1958) Pigments and photosynthesis in a carotenoid-deficient mutant of
1188 Chlamydomonas. Nature **182:** 98-100

1189 **Schmid LM, Manavski N, Chi W, Meurer J** (2024) Chloroplast Ribosome Biogenesis Factors.
1190 Plant Cell Physiol **65:** 516-536
1191 **Schmollinger S, Chen S, Strenkert D, Hui C, Ralle M, Merchant SS** (2021) Single-cell
1192 visualization and quantification of trace metals in Chlamydomonas lysosome-related
1193 organelles. Proc Natl Acad Sci U S A **118**
1194 **Schneider D, Lopez LS, Li M, Crawford JD, Kirchhoff H, Kunz HH** (2019) Fluctuating light
1195 experiments and semi-automated plant phenotyping enabled by self-built growth racks and
1196 simple upgrades to the IMAGING-PAM. Plant Methods **15:** 156
1197 **Schwartz S, Engstler C, Mühlbauer S, Windenbach E, Wunder T, Kunz HH, Brandt B**
1198 (2025) Catch & Release-rapid cost-effective protein purification from plants using a DIY
1199 GFP-Trap-protease approach. Plant J **124:** e70544
1200 **Simms D, Cizdziel PE, Chomczyński PA** (1993) TRIzol: A new reagent for optimal single-step
1201 isolation of RNA. *In*,
1202 **Small I, Melonek J, Bohne AV, Nickelsen J, Schmitz-Linneweber C** (2023) Plant organellar
1203 RNA maturation. Plant Cell **35:** 1727-1751
1204 **Stöberl S, Balles M, Kellerer T, Rädler JO** (2023) Photolithographic microfabrication of
1205 hydrogel clefts for cell invasion studies. Lab Chip **23:** 1886-1895
1206 **Strassert JFH, Irisarri I, Williams TA, Burki F** (2021) Author Correction: A molecular
1207 timescale for eukaryote evolution with implications for the origin of red algal-derived
1208 plastids. Nat Commun **12:** 3574
1209 **Sueoka N** (1960) MITOTIC REPLICATION OF DEOXYRIBONUCLEIC ACID IN
1210 CHLAMYDOMONAS REINHARDI. Proc Natl Acad Sci U S A **46:** 83-91
1211 **Sumiya N, Fujiwara T, Era A, Miyagishima SY** (2016) Chloroplast division checkpoint in
1212 eukaryotic algae. Proc Natl Acad Sci U S A **113:** E7629-e7638
1213 **Sun L, Ge Y, Sparks JA, Robinson ZT, Cheng X, Wen J, Blancaflor EB** (2019) TDNAscan:
1214 A Software to Identify Complete and Truncated T-DNA Insertions. Front Genet **10:** 685
1215 **Supek F, Bošnjak M, Škunca N, Šmuc T** (2011) REVIGO summarizes and visualizes long lists
1216 of gene ontology terms. PLoS One **6:** e21800
1217 **Theis J, Niemeyer J, Schmollinger S, Ries F, Rütgers M, Gupta TK, Sommer F, Muranaka**
1218 **LS, Venn B, Schulz-Raffelt M, Willmund F, Engel BD, Schroda M** (2020) VIPP2
1219 interacts with VIPP1 and HSP22E/F at chloroplast membranes and modulates a retrograde
1220 signal for HSP22E/F gene expression. Plant Cell Environ **43:** 1212-1229
1221 **Tulin F, Cross FR** (2014) A microbial avenue to cell cycle control in the plant superkingdom.
1222 Plant Cell **26:** 4019-4038
1223 **Umen JG, Goodenough UW** (2001) Control of cell division by a retinoblastoma protein homolog
1224 in Chlamydomonas. Genes Dev **15:** 1652-1661
1225 **Urrego D, Tomczak AP, Zahed F, Stühmer W, Pardo LA** (2014) Potassium channels in cell
1226 cycle and cell proliferation. Philos Trans R Soc Lond B Biol Sci **369:** 20130094
1227 **Vercruyssen L, Tognetti VB, Gonzalez N, Van Dingenen J, De Milde L, Bielach A, De Rycke**
1228 **R, Van Breusegem F, Inzé D** (2015) GROWTH REGULATING FACTOR5 stimulates
1229 Arabidopsis chloroplast division, photosynthesis, and leaf longevity. Plant Physiol **167:**
1230 817-832
1231 **Vilarrasa-Blasi J, Vellosillo T, Jinkerson RE, Fauser F, Xiang T, Minkoff BB, Wang L,**
1232 **Kniazev K, Guzman M, Osaki J, Barrett-Wilt GA, Sussman MR, Jonikas MC,**
1233 **Dinneny JR** (2024) Multi-omics analysis of green lineage osmotic stress pathways unveils
1234 crucial roles of different cellular compartments. Nat Commun **15:** 5988

1235 **Walther P, Ziegler A** (2002) Freeze substitution of high-pressure frozen samples: the visibility of
1236 biological membranes is improved when the substitution medium contains water. J Microsc
1237 **208:** 3-10
1238 **Wang P, Robert L, Pelletier J, Dang WL, Taddei F, Wright A, Jun S** (2010) Robust growth of
1239 Escherichia coli. Curr Biol **20:** 1099-1103
1240 **Wu FH, Shen SC, Lee LY, Lee SH, Chan MT, Lin CS** (2009) Tape-Arabidopsis Sandwich - a
1241 simpler Arabidopsis protoplast isolation method. Plant Methods **5:** 16
1242 **Wunder T, Brandt B, Kramer L, Kunz H-H** (2025) RNAseq of ribo-depleted RNA from light
1243 treated WT and kea Chlamydomonas. *In*, NCBI Sequence Read Archive (SRA)
1244 **Xu F, Pan J** (2020) Potassium channel KCN11 is required for maintaining cellular osmolarity
1245 during nitrogen starvation to control proper cell physiology and TAG accumulation in
1246 Chlamydomonas reinhardtii. Biotechnol Biofuels **13:** 129
1247 **Zhang Z, Shrager J, Jain M, Chang CW, Vallon O, Grossman AR** (2004) Insights into the
1248 survival of Chlamydomonas reinhardtii during sulfur starvation based on microarray
1249 analysis of gene expression. Eukaryot Cell **3:** 1331-1348

1250